NAA-SR-5416
REACTOR TECHNOLOGY
65 PAGES

KINETIC EXPERIMENTS ON WATER BOILERS – "A" CORE REPORT – PART II, ANALYSIS OF RESULTS

Compiled by M. Dunenfeld from the writings and analyses
of D. L. Hetrick, D. P. Gamble, A. Norman,
E. R. Cohen, M. Dunenfeld, R. E. Wimmer,
and A. Schwarz

ATOMICS INTERNATIONAL

A DIVISION OF NORTH AMERICAN AVIATION, INC.
P.O. BOX 309 CANOGA PARK, CALIFORNIA

CONTRACT: AT(11-1)-GEN-8
ISSUED: FEB 1962

DISCLAIMER

DISTRIBUTION

This report has been distributed according to the category "Reactor Technology" as given in "Standard Distribution Lists for Unclassified Scientific and Technical Reports" TID-4500 (16th Ed.), December 15, 1960. A total of 650 copies was printed.

ACKNOWLEDGMENT

In compiling the material in this report I have drawn freely from the work of the individuals credited. I would like to apologize to my colleagues for any statements I have thus made in their names with which they might take issue and assume full responsibility for any failings in the presentation.

I wish to acknowledge also the efforts of others involved directly with or providing services to the KEWB program, and without which our analysis of the reactor could not have proceeded: namely, J.W. Flora, M.E. Remley, and M. Silberberg for their able direction and inspiration; R.K. Stitt, J.H. Roecker, and the KEWB staff who have conducted the experimental effort; H.P. Flatt, L.R. Blue, R. Mikell, and J. Richardson of Numerical Analysis who create our computer programs and make them work; and L.P. Shaw, E. McKenzie, and J. Buchinsky who managed the data processing.

Especially do I thank E.R. Cohen for his comprehensive review of this document.

M. Dunenfeld

CONTENTS

TABLE

FIGURES

ABSTRACT

This report is a summary of the status of the analytic portion of the KEWB program at the time of completion of the spherical core experiments.

Three computer programs have been developed for use in this analytic effort. The first reassembles and smooths three decades of reactor power data read separately from oscillogram records of reactor excursions. It then computes the logarithmic derivative of the power, energy release, fuel solution temperature, and temperature compensated reactivity. The second program utilizes the space-independent neutron kinetics equations with any number of delayed neutron groups to determine the reactivity in the reactor from the power and its derivative. The third program solves the space-independent kinetics equations for the neutron flux from an input reactivity or initial period. Up to 50 reactivity feedback equations including delayed neutrons are provided for in this program.

A mathematical model of the reactor investigated extensively was one containing six delayed neutron groups, conventional treatment of temperature reactivity compensation, and void compensation of reactivity induced by radiolytic gas void growth proportional to the product of reactor power and energy release. Partial mathematical solutions to the kinetic equations were derived for reactivity feedback proportional to prompt temperature and void growth according to the product of power and energy. These solutions apply where delayed neutrons can be neglected, which is the region of major interest. Expressions are available relating power and energy and defining the peak power and energy release to peak power in terms of basic reactor parameters.

Experimental evidence, particularly the experimental inhour curve, of another reactivity influencing mechanism was found present in the reactor at periods shorter than 10 msec. This mechanism has been shown to behave as a delayed neutron group, having a mean delay time of approximately 2 msec and an abundance of 2%. A plausible origin of such neutrons has been shown to be the reflector which thermalizes core neutrons and returns them to the core following a delay.

Ramp induced transients characterized by their minimum period show behavior which is essentially the same as step induced transients, with the same initial period. These transients provide an approximate means of verification of the value of the apparent neutron lifetime divided by the effective delayed neutron fraction.

I. INTRODUCTION

The Kinetic Experiments on Water Boilers (KEWB) program was initiated by Atomics International under contract to the Atomic Energy Commission in October, 1954. The objective of the program is to establish a firm basis for the evaluation of the safety of aqueous homogeneous reactor designs with regard to an accidental release of large amounts of reactivity. Engineering data produced by the KEWB reactor to date have demonstrated the inherent safety of this type of reactor under the widest variety of operating conditions. These data are presented in detail in Part I of this report, which has been published separately.[1]

Analysis of the data produced by the KEWB reactor has been oriented toward the establishment, in terms of basic reactor parameters, of a clear understanding of the phenomena which shut down water boiler reactor excursions. This will make it possible to evaluate the potential hazards of the reactor type in general, and of specific designs differing in configuration from those for which the engineering data are available. This document presents the status of the analytic portion of the KEWB program at the time of completion of the spherical core experiments, which involve more than 900 power excursions.

The KEWB reactor spherical core ("A" core) is a 12-in. ID stainless steel vessel with 0.25-in. -thick walls. It was operated with a graphite reflector approximately 2 ft thick radially. Two core loadings were studied in detail: one with the vessel 85% full (underfull core), and the other with the vessel full to the 2-in. -diameter tubular neck at the top of the sphere. The fuel was 93% enriched UO_2SO_4 in 0.1 molar H_2SO_4 solution, with loadings of 2043 and 1533 grams of uranium in the underfull and full core respectively. Corresponding fuel volumes were 11.3 and 13.6 liters. More detailed descriptions of the reactor and facility can be found in the companion report[1] mentioned previously.

II. DEVELOPMENT OF NUMERICAL DATA REDUCTION SYSTEM AND COMPUTER CODES

Three digital computer programs have been developed for use in the analysis of KEWB behavior. Two are used in reduction of the experimental data, the third in evaluation of mathematical models of the reactor. The first, in conjunction with oscillogram reading procedures, synthesizes and smooths the numerical power data. It also computes energy release and reciprocal period. The second program computes the system reactivity from the power and the space-independent kinetics equations. The third computes a power burst from an input reactivity with space-independent reactor kinetics equations containing terms descriptive of the reactivity feedback mechanisms.

A. REDUCTION OF OSCILLOGRAM RECORDS OF INSTANTANEOUS POWER TO NUMERICAL DATA, AND CALCULATION OF ENERGY RELEASE AND RECIPROCAL PERIOD

1. Statement of the original problem, the solution employed, and difficulties encountered.

Three channels of the reactor power having sensitivity ratios of approximately 100:10:1 are recorded in order to obtain three decades of information about KEWB transients. Duplicate channels are also recorded in order to provide crosscheck and also one complete set of data in the event of the failure of some channel. A reproduction of a typical oscillogram is shown in Figure 1. These power data are required in numerical form for the analytical effort in computing energy release, reciprocal period and reactivity, and for comparison or burst shape produced by mathematical models. The data reduction problem initially formulated was to obtain numerical data from the oscillograms, join the three channels of data, average duplicate sets, and compute the reciprocal period and energy release at each power point. The reciprocal period is defined as the logarithmic derivative of the power curve.

In order to handle the volume of data involved, a digital computer program, TRADE (Transient Analysis Drudgery Eliminator), was developed to perform the data reduction in conjunction with cards from numerical readout of the oscillogram data. The oscillograms are read in arbitrary deflection units as a function of constant (for any transient) time increments, both sets of power traces being read at the same time points if all the channels of both sets of

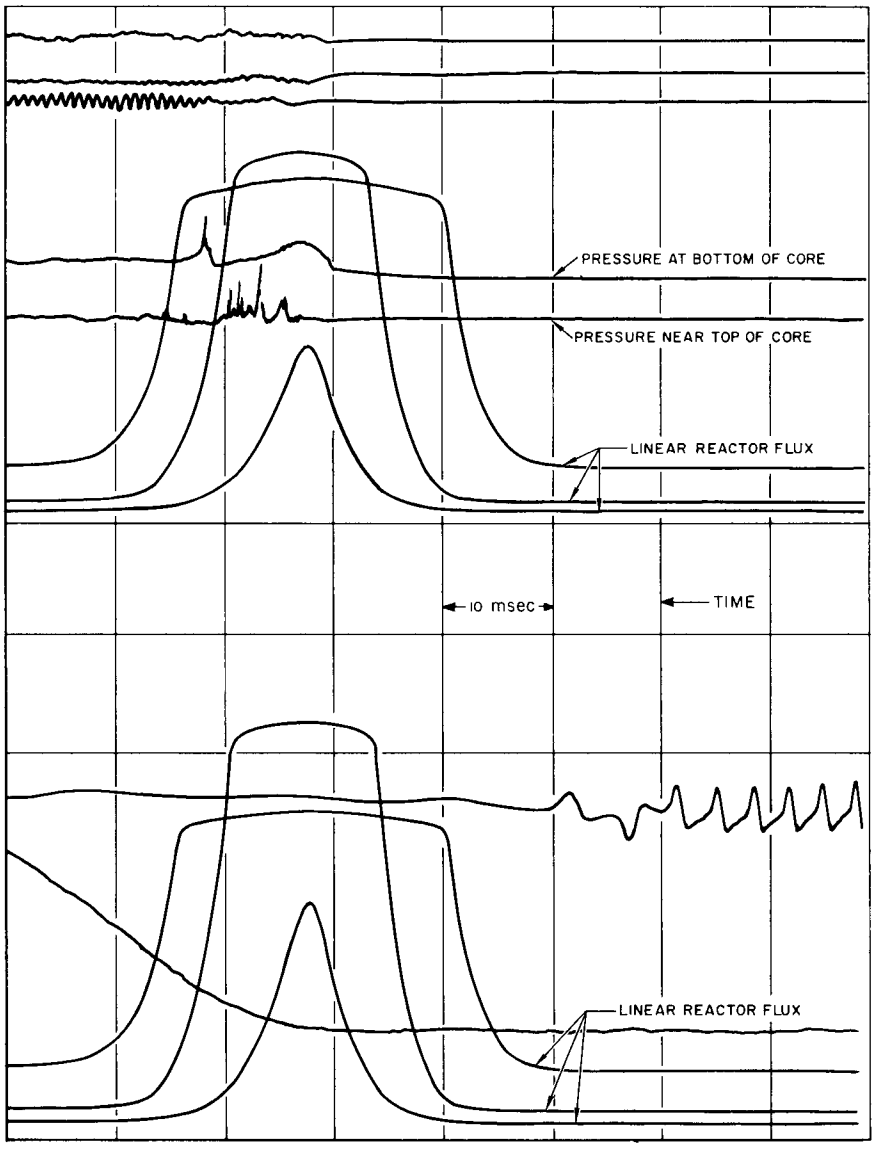

Figure 1. Typical Oscillogram-Transient No. 219B

data are usable. If not, the functioning channels of each set are read, provided one of them is the channel recording the power peak. About 100 points are read for each set of power channels.

The computer is programmed by TRADE to detect the discontinuities in deflection which arise from the termination of one power channel and the beginning of the following. This establishes identity of the channels. Factors are computed which join the endpoints (both read at the same time-point) of adjacent channels, forming a continuous set of data proportional to power. These factors

are not necessarily the same in joining the ascending and descending sections of a channel to the rest of the data. This has been the case particularly for the least sensitive channel which reads the power peak. Neither the precise reason for this behavior nor its effect on the shape of the burst has yet been determined.

The value of the power at the peak for each set of power channels, read into the computer as input information, is employed to convert the continuous set of deflection data into coolant thermal power units. Coolant thermal power is defined as the rate of sensible heat deposition in the core during equilibrium operation of the reactor at constant low power, because the ion chambers must be calibrated under these conditions. The second set of power data is subjected to the same procedure, and the two sets are averaged at each time point. From the averaged power the reciprocal period, ω, is computed using the bridging two-point log-derivative formula,

$$\omega(t) = \frac{\ell n\, N_{t+1} - \ell n\, N_{t-1}}{2\Delta t} \qquad \ldots(1)$$

where N = power and t = time, in regions where ω is changing rapidly. A bridging interval of ± 3 time increments is used in regions where ω is changing very slowly. This latter expedient partially removes some of the line frequency and other nonrandom noise which affects two or three successive points in the same direction. The selection of the bridging interval is not made by the program, but must be written into the input information for each transient by the individual who processes the transient data.

The energy release at the initial time point is calculated assuming the power has been rising exponentially for several preceding periods. If the power is negligibly small but not zero at the beginning of the exponential rise, the energy released to time t_1 can be found as follows:

$$N = N_o e^{\omega t} \qquad \ldots(2)$$

$$E_{t_1} = \int_o^{t_1} N dt = N_o \int_o^{t_1} e^{\omega t} dt \qquad \ldots(3)$$

$$= \frac{N_o}{\omega}\left(e^{\omega t_1} - 1\right) = \frac{N_{t_1}}{\omega} - \frac{N_o}{\omega} \simeq \frac{N_{t_1}}{\omega} \qquad \ldots(4)$$

E(t) for the rest of the transient is obtained by accumulating ΔE increments calculated with a simple 2-point trapezodial integration. TRADE was used for more than a year. Results were reasonably satisfactory, except that the reciprocal period computed was excessively noisy in many transients. This was a consequence of the amplification of noise by numerical differentiation. There are a number of potential sources of noise in the raw data, such as line frequency interference and electronic malfunction recorded on the oscillogram, distortion of the oscillogram in photographic processing and storage, errors in setting base lines for taking readings, and random reading errors. The amount of scatter this introduced in the reactivity computation, which is a major justification for the numerical reduction in the first place, was large enough to make it questionable as to where to draw a reasonable curve through the plotted reactivity data. It was therefore decided to incorporate some means of smoothing the power data and computed reciprocal period into the data reduction code.

2. Revised Data Reduction Requirements and the Smoothing Code.

Besides incoporating smoothing into the data processing code, it was decided to change a few other features of the system to improve results.

The process of averaging the two sets of power data for a transient was eliminated because a bad set of data might better be located if treated individually. When two sets exist, each is now processed separately.

In joining two channels of data with TRADE, any error in the last point of a channel affects all the subsequent points because the normalization factor is determined at one time point only. The system which replaced this makes use of overlapping power data for three successive time-points. Three normalization factors are computed, the average of which is used to join the channels.

The broadest statement of the requirements of a data smoothing code would be to fit a curve to a set of points much as would be done by a skilled person with a set of ships curves. The general problem, however, of coding the conditions used and decisions made by the mind in curve fitting was considered too complex to be supported by the KEWB project.

After only partially successful trials with polynomial curve-fitting to individual sections of the data before joining, and smoothing formulas applied to each point and its three to five neighbors on either side, reasonably satisfactory smoothing was developed based upon a code located in the SHARE library.[2] The code developed first tests all but 5 points at either end of the data set for "wildness" by fitting a quadratic to the point in question and to the five adjacent points on either side. If the fit is very poor, the point is considered wild, and replaced with the quadratic fit. Smoothing is performed in a similar manner, all the points except the five beginning and end-points of a set being smoothed three times, and being replaced at the end of each pass with the value of the quadratic fit to the point in question and the five adjacent points on either side. The end-points are replaced with the values of a cubic fit to the first or last eleven points. They are carried through the computation in this manner, but are not a good reflection of real data, and are ignored in the final results. The logarithmic derivatives are computed from the derivatives of the polynomials found in the final pass of smoothing.

Figure 2 shows the reciprocal period, which is the best measure of the smoothness of the power, computed with and without smoothing. The derivative computed from the smoothed power falls far short of the ideal, but permits drawing of a smoothed curve with relative ease, whereas it would be extremely difficult to decide where the curve lay from the derivative computed without smoothing. The degree of smoothing employed, although mild from the stand-

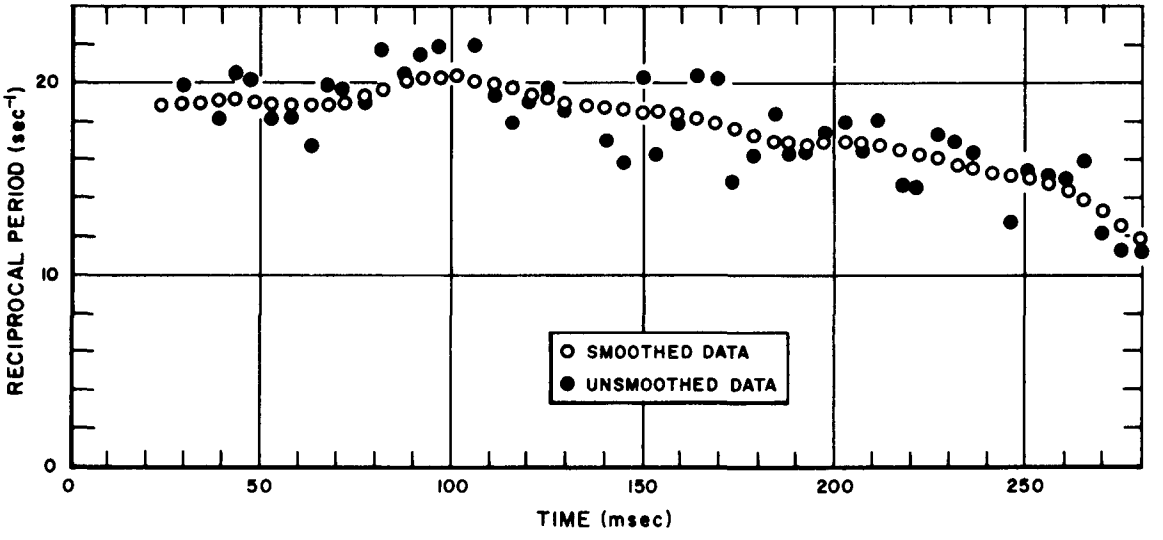

Figure 2. Reciprocal Period, Smoothed and Unsmoothed Logarithmic Derivative of Neutron Flux

point of the ultimate, does not distort the power trace appreciably. In contrast, when the number of cycles of smoothing, which is three in the system adopted, was increased to ten, the value of peak power was reduced 5% by smoothing.

The computation of reactivity, discussed in the following section, formerly performed separately with card output from TRADE, has been incorporated into the data reduction code. A block diagram of the data reduction system is included as Figure 3.

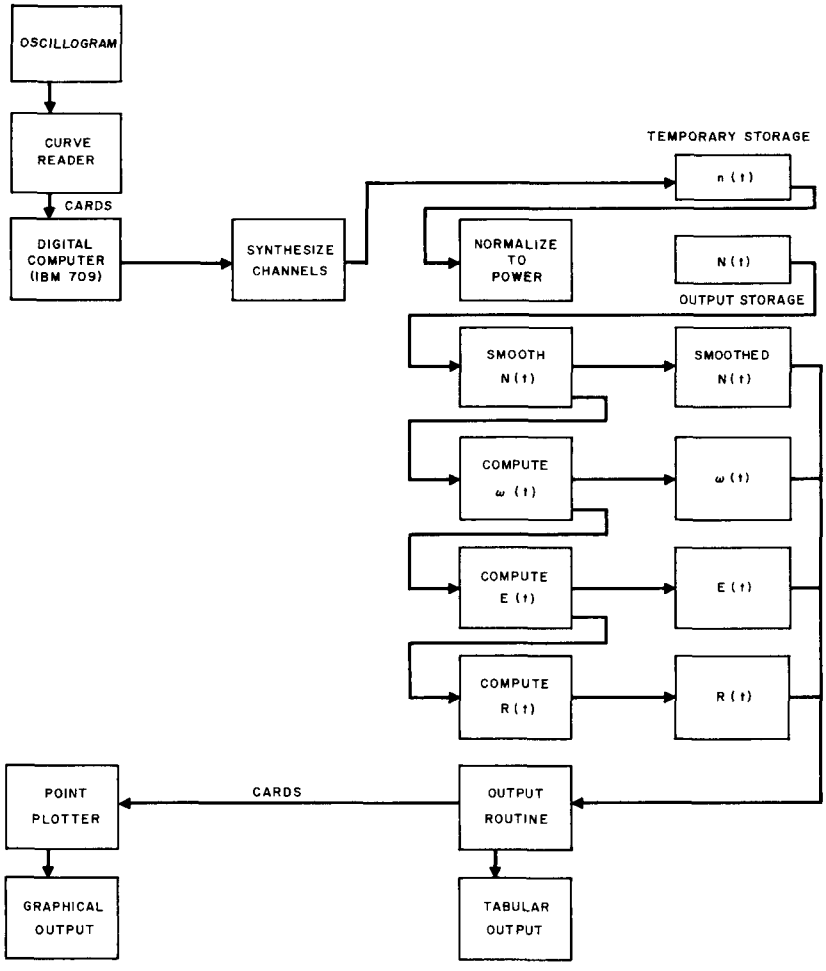

Figure 3. KEWB Numerical Data Reduction System

B. COMPUTATION OF REACTIVITY

The computer program for the computation of reactivity was written to conform with the following mathematical treatment:*

*The remainder of this section was written by Dr. E.R. Cohen.

The space-independent reactor kinetics equations are

$$\frac{dN}{dt} = \frac{\beta}{\ell}(R - 1)N + \sum f_i W_i \qquad \ldots(5)$$

$$\frac{dW_i}{dt} = \lambda_i(N - W_i) \qquad \ldots(6)$$

where

N = instantaneous neutron density of power,

t = time,

β = effective delayed neutron fraction,

ℓ = effective core neutron lifetime,

R = instantaneous reactivity in dollars.

R_o = input reactivity,

f_i = relative yield of the i^{th} delayed neutron precursor group,

W_i = relative concentration of the i^{th} delayed neutron precursor group, and

λ_i = decay constant for the i^{th} delayed neutron precursor group.

We can rearrange Equation 5 and solve for the reactivity, R,

$$R(t) = \frac{\ell}{\beta}\omega(t) + 1 - \frac{1}{N(t)}\sum f_i W_i(t) \qquad \ldots(7)$$

where $\omega(t) = \frac{1}{N}\frac{dN}{dt}$ is the apparent instantaneous inverse period. Furthermore, Equation 6 can be integrated to give

$$W_i(t) = W_i(t_o)e^{-\lambda_i(t-t_o)} + \int_{t_o}^{t} \lambda_i N(t')e^{-\lambda_i(t-t')}dt' \qquad \ldots(8)$$

The data available to us are the values of N(t) at a set of points equally spaced in time with an interval h.

We must develop an expression for $W_{i,k}$ from Equation 8, where the subscript k indicates the value of the variable at the k^{th} time-point, that is, at the time t = kh. D. L. Hetrick in a previous analysis[3] expanded N(t') in Equation 8 in a Taylor series and integrated term by term.

The practical difficulty arises in evaluating the various derivatives numerically from the given set of points. One procedure is to make a quadratic fitting to N(t') at three sucessive points and integrate from $t_o = t - 2h$ up to t. If we now write a new variable $\tau = t - t'$, Equation 8 becomes

$$W_{i,k} = W_{i,k-2}e^{-2h\lambda_i} + \lambda_i\int_o^{2h} N(t-\tau)e^{-\lambda_i\tau}\,d\tau \qquad \ldots(9)$$

The second order Lagrangian interpolation formula for $N(t - \tau)$ can be written

$$N(t-\tau) = \frac{1}{2h^2}\left[\tau(\tau - h)N_{k-2} + 2\tau(2h - \tau)N_{k-1} + (h - \tau)(2h - \tau)N_k\right]$$

$$= N_k + \frac{\tau}{2h}(4N_{k-1} - N_{k-2} - 3N_k) + \frac{\tau^2}{2h^2}(N_{k-2} - 2N_{k-1} + N_k) \qquad \ldots(10)$$

This same expression can be obtained, however, if we make a Taylor expansion about the midpoint of the integration interval; i.e., about the point $\tau = h$. We write

$$N(t-\tau) = N_{k-1} + (\tau - h)N' + \frac{1}{2}(\tau - h)^2N'' + \ldots \qquad \ldots(11)$$

and use the approximations

$$N' = (N_{k-2} - N_k)/2h \qquad \ldots(12)$$

$$N'' = (N_{k-2} - 2N_{k-1} + N_k)/h^2 \qquad \ldots(13)$$

then

$$N(t - \tau) = N_{k-1} + \frac{(\tau - h)}{2h}(N_{k-2} - N_k) + \frac{(\tau - h)^2}{2h^2}(N_{k-2} - 2N_{k-1} + N_k) + \ldots\ldots(14)$$

and this expression can be readily shown to be equivalent to Equation 10. Therefore, the Lagrangian quadratic fit is equivalent to a Taylor expansion about the midpoint followed by an appropriate second order approximation to the derivatives.

The next step is to introduce Equation 10 into the expression for $W_{i,k}$. For $k \geq 2$ we can write

$$W_{i,k} = W_{i,k-2}e^{-2h\lambda_i} + \int_o^{2h} \lambda_i e^{-\lambda_i \tau}\left[N_k - \frac{\tau}{2h}(3N_k - 4N_{k-1} + N_{k-2})\right.$$

$$\left. + \frac{\tau^2}{2h^2}(N_k - 2N_{k-1} + N_{k-2})\right] d\tau \qquad \ldots(15)$$

The integrals in Equation 8 may be easily evaluated:

$$\int_o^{2h} \lambda_i e^{-\lambda_i \tau} d\tau = 1 - e^{-2h\lambda_i}$$

$$\int_o^{2h} \frac{\lambda_i \tau}{2h} e^{-\lambda_i \tau} d\tau = \frac{1}{2h\lambda_i}\left[1 - (1 + 2h\lambda_i)e^{-2h\lambda_i}\right]$$

$$\int_o^{2h} \frac{\lambda_i^2}{2h^2} e^{-\lambda_i \tau} d\tau = \frac{1}{2h^2\lambda_i^2}\left[2 - (2 + 4h\lambda_i + 4h^2\lambda_i^2)e^{-2h\lambda_i}\right],$$

so that

$$W_{i,k} = W_{i,k-2}e^{-2h\lambda_i} + N_k\left(1 - e^{-2h\lambda_i}\right)$$

$$-\frac{1}{2h\lambda_i}(3N_i - 4N_{k-1} + N_{k-2})\left(1 - e^{-2h\lambda_i} - 2h\lambda_i e^{-2h\lambda_i}\right)$$

$$+\frac{1}{2h^2\lambda_i^2}(N_k - 2N_{k-1} + N_{k-2})\left(2 - 2e^{-2h\lambda_i} - 4h\lambda_i e^{-2h\lambda_i} - 4h^2\lambda_1^2 e^{-2h\lambda_i}\right)$$

This expression can be regrouped in terms of the N_k to give us

$$W_{i,k} = W_{i,k-2}e^{-u_i} + \frac{N_k}{u_i^2}\left[4 - 3u_i + u_i^2 - (4 + u_i)e^{-u_i}\right]$$

$$+ \frac{4N_{k-1}}{u_i^2}\left[(2 + u_i)e^{-u_i} - 2 + u_i\right]$$

$$+ \frac{N_{k-2}}{u_i^2}\left[4 - u_i - (4 + 3u_i + u_i^2)e^{-u_i}\right] \qquad \ldots(16)$$

where $u_i = 2h\lambda_i$.

In general, particularly for a fast transient, u will be a number much smaller than unity and it is therefore not only useful from a computational point of view, but also instructive to expand the square brackets in Equation 16 into power series in u.

We then find

$$\frac{1}{u^2}\left[4 - 3u + u^2 - (4 + u)e^{-u}\right] = \frac{u}{6}\left[1 - \frac{u^2}{20} + \frac{u^3}{60} + \ldots\right] \qquad \ldots(17)$$

$$\frac{1}{u^2}\left[(2+u)e^{-u} - 2 + u\right] = \frac{u}{6}\left[1 - \frac{u}{2} + \frac{3u^2}{20} - \frac{u^3}{30} + \ldots\right] \qquad \ldots(18)$$

$$\frac{1}{u^2}\left[4 - u - (4 + 3u + u^2)e^{-u}\right] = \frac{u}{6}\left[1 - u + \frac{9}{20}u^2 - \frac{2}{15}u^3 + \ldots\right] \qquad \ldots(19)$$

and we can see that the first term corresponds to a Simpson's Rule integration. Equation 16 can then be written

$$W_{1,k} = W_{1,k-2}e^{-u_1} + \frac{u_1}{6}\left(N_k + 4N_{k-1} + N_{k-2}\right)$$

$$- \frac{u_1^2}{6}\left(2N_{k-1} + N_{k-2}\right)$$

$$+ \frac{u_1^3}{120}\left(-N_k + 12N_{k-1} + 9N_{k-2}\right)$$

$$- \frac{u_1^4}{360}\left(8N_{k-2} + 8N_{k-1} - N_k\right) + \ldots$$

or finally,

$$W_{1,k} = W_{1,k-2} + \frac{u_1}{6}\left(N_k + 4N_{k-1} + N_{k-2} - 6W_{1,k-2}\right)$$

$$- \frac{u_1^2}{6}\left(2N_{k-1} + N_{k-2} - 3W_{1,k-2}\right)$$

$$+ \frac{u_1^3}{120}\left(-N_k + 12N_{k-1} + 9N_{k-2} - 20W_{1,k-2}\right)$$

$$- \frac{u_1^4}{360}\left(-N_k + 8N_{k-1} + 8N_{k-2} - 15W_{1,k-2}\right) + \ldots \qquad \ldots(20)$$

It should not be forgotten that Equation 16 and 20 are analytically equivalent, since Equation 20 is merely the power series expansion of Equation 16. The importance of Equation 20 arises from the computational difference between the two expressions. For small values of u_i there is a strong cancellation of terms, and hence a serious loss of significant figures. This loss can be avoided only if, in these cases, the power series expansion of the right-hand side of Equations 17 through 19 are used in place of direct evaluation of the left side. We can evaluate the point at which the left side is more accurate than the right.

For Equation 17, the error in the left-hand side due to the finite number of bits carried in the calculation on the IBM 709 is approximately $\frac{4}{u^2}2^{-27}$. The error in the right-hand side of Equation 17 is a result of omitting the term $-u^5/1680$. These two expressions will be equal in magnitude when $6720.2^{-27} = u^7$, and hence u = 0.24. For Equation 18, the error in the left-hand side is $\frac{2}{2u^2} \times 2^{-27}$, while the error in the right-hand side is $+u^5/1008$, and the equality is $u^7 = 2016.2^{-27}$ or u = 0.20. For Equation 19, the left-hand error is $\frac{-4}{u^2} \times 2^{-27}$, while the right hand error is $5u^5/1008$; and this leads to the break-even point given by $u^7 = \frac{4032}{5}2^{-27}$, or u = 0.18. Hence we can quite readily place the break-point at u = 0.20; for smaller values of u, we can use the right-hand side of Equations 17 through 19; for larger values of u_i, one would use the left-hand side.* With this split in calculation formula we can insure that the accuracy of the calculation will be of the order of a few parts in 10^6 or better, consistently throughout the entire range of the variable. If we wished to retain only through the quadratic term in Equation 17 through 19, a similar analysis could tell us the break-point and the maximum accuracy in this case also. (For a calculation which keeps only up to u^3 in Equation 20 and neglects the term in u^4, we find a break-point u = 0.125 and a maximum accuracy of 10^{-5}, which is in fact probably adequate for most calculations.)

Therefore one should use either Equations 16 or 20 to calculate $W_{i,k}$, depending on the value of u_i. These values of $W_{i,k}$ are then inserted into Equation 7 to give the reactivity.

*Equivalently, for $u_i \leq 0.20$, we should use Equation 6 to calculate $W_{i,k}$; for $u_i > 0.20$, we should use Equation 8.

Actually, Equations 16 and 20 can be used only for $k \geq 2$, since we are carrying out a two-step integration; we still require a method for starting the integration. This is most easily done by assuming that the transient has been initiated at very low power and that the reactor has reached a stationary, asymptotic period prior to the time at which data have been taken. One can then use the observed initial period $\omega(o)$ and assume that the delayed neutron precursors are in equilibrium with this asymptotic condition. Under this assumption we can write

$$W_{i,o} = \frac{\lambda_i N_o}{\lambda_i + \omega(o)} \qquad \ldots(21)$$

$$W_{i,1} = \frac{\lambda_i N_1}{\lambda_i + \omega(o)} \qquad \ldots(22)$$

C. NUMERICAL SOLUTIONS TO REACTOR KINETICS EQUATIONS

In order to permit evaluation of mathematical models of the KEWB behavior, a computer program to solve the space-independent reactor kinetics equations was deemed necessary; for, in general, analytic solutions to the equations are not possible when the reactivity feedback equations are complex. This need has been filled with the Atomics International Reactor Kinetics Code (AIREK).*[4]

The set of equations solved follows

$$\frac{dN}{dt} = \frac{\rho(t) - \beta}{\ell} N(t) + \sum_{i-1}^{J} \lambda_i C_i(t) + S_o J \leq 20 \qquad \ldots(23)$$

$$\rho(t) = \text{fnct.}\ (t, N, T_m \ldots\ldots) \qquad \ldots(24)$$

$$\frac{dC_i}{dt} = \frac{\beta f_i}{\ell} N(t) - \lambda_i C_i(t) \qquad \ldots(25)$$

$$\frac{dT_m}{dt} = E_m N(t) - F_m N_o - G_m T_m(t) \qquad \ldots(26)$$

*The remainder of this section was taken from the referenced paper by A. Schwarz.

where N(t) is the neutron flux at time t, ρ (t) is the total reactivity at time t, β is the total fraction of delayed neutrons; ℓ is the neutron lifetime, f_i are the relative yields for each delayed group, λ_i are the feedback coefficients for each delayed neutron group, C_i are the delayed neutron concentrations; and S_o is the constant source term. The feedback variables $T_m(t)$ are represented as simple linear differential equations with arbitrary constant coefficients E_m, F_m, G_m, and $N_o = N(O)$. The maximum number of variables that can be solved for is 50. By making the following substitutions,

$$\frac{\rho(t)}{\beta} = r(t) \qquad \ldots(27)$$

where r(t) is the total reactivity in dollars at time t, and

$$\frac{\beta f_i}{\ell \lambda_i} W_i(t) = C_i(t) \qquad \ldots(28)$$

where $W_i(t)$ are the normalized delayed neutron concentrations. Equations 23 and 25 become

$$\frac{dN}{dt} = \frac{\beta}{\ell}(r(t) - 1)N(t) + \frac{\beta}{\ell}\left[\sum_{i=1}^{J} f_i W_i(t) + S^*\right] \qquad \ldots(29)$$

where $S^* = \frac{\ell}{\beta} S_o$, and

$$\frac{dW_i}{dt} = -\lambda_i W_i(t) + \lambda_i N(t). \qquad \ldots(30)$$

Equations 26 and 30 can now be combined into one logical form:

$$\frac{dX_n}{dt} = -M_n X_n(t) + K_n N(t) - L_n N_o \qquad \ldots(31)$$

where $L_n = O$ for all delayed neutron groups. Equations 29 and 31 are the actual equations solved by this code.

The following is a mathematical description of the numerical description of the numerical method of integration developed by E. R. Cohen, based upon the Fourth-order Runge-Knutta Integration formulae.

We will collect terms in the differential equations solved in such a manner that the differential equations now have the following form:

$$\frac{dV}{dt} = \alpha_o V(t) + R(t), \qquad \ldots(32)$$

where α_o is the sum of all the coefficients of V(t) at the beginning of the interval h and, R(t) is the sum of all the rest of the terms in the differential equation. We will define V_o as the value of V, and R_o as the value of R, at the beginning of the interval h.

We now compute the following:

$$\Delta 1 = \frac{h}{2} C_1(x)(\alpha_o V_o + R_o) \qquad \ldots(33)$$

where $x = \alpha_o \frac{h}{2}$, and

$$C_1(x) = \frac{e^x - 1.0}{x}$$

$$C_2(x) = \frac{C_1(x) - 1.0}{x}$$

$$C_3(x) = \frac{2C_2(x) - 1.0}{x}$$

where e is the base of the natural logarithms.

$$V_a = V_o + \Delta_1 \qquad \ldots(34)$$

where V_a is a first approximation of the value of V(t) at $\frac{h}{2}$. Using V_a in place of V_o in the differential equations we find a value for R_a and then compute:

$$\Delta_2 = \frac{h}{2} C_2(x)(R_a - R_o) + \Delta_1 \qquad \ldots(35)$$

$$V_o = V_o + \Delta_2 \qquad \ldots(36)$$

where V_b is the corrected value of V at the half-interval $\frac{h}{2}$. Replacing V_a with V_b in the differential equation, we find a value for R_b and compute

$$\Delta_3 = h\left[2C_2(x')(R_b - R_o) + C_1(x')(\alpha_o V_o + R_o)\right] \qquad \ldots(37)$$

where $x' = \alpha_o h$, .

$$V_c = V_o + \Delta_3 \qquad \ldots(38)$$

where V_c is the first approximation of the value of V at the end of the interval h.

Replacing V_b with V_c, we find a value for R_c and compute

$$\Delta_4 = h\left\{\left[2C_3(x') - C_2(x')\right](R_o - 2R_b + R_c)\right\} + \Delta_3 \qquad \ldots(39)$$

$$V_1 = V_o + \Delta_4 \qquad \ldots(40)$$

where V_1 is the corrected value of V at the end of the interval h.

In order to reduce computation time, it is important that the interval h be as large as possible consistent with the preservation of accuracy. We define the quantities $\bar{\omega}$ and Q;

$$\bar{\omega} = \frac{1}{h} \ell n \frac{N_1}{N_o} \qquad \ldots(41)$$

$$Q = \frac{hC_2(\alpha_o h)}{1 + C_i(\alpha_o h)} \omega_{io} - 2\bar{\omega} + \omega_{il} \qquad \ldots(42)$$

where ω_{io} is the instantaneous inverse period at the beginning of the interval h, and ω_{il} is the instantaneous inverse period at the end of the interval h, and α_o is the value of α for the neutron density equation

$$\left[\alpha_o h = \frac{\beta}{\ell} h(r_o - 1)\right].$$

The following are the various conditions under which the interval h will be either expanded or contracted for further computations.

1) If, for all i, $\Delta_{1i} < 2^{-14} V_{oi}$ and $Q \geq Q_1$, the program continues the calculation with the same interval h for the next step.

2) If, for all i, $\Delta_{1i} < 2^{-14} V_{ci}$ and $Q < Q_1$, the program finishes the calculation of the next point with its original interval h but for the next point uses $h' = \sqrt{2} \cdot h$.

3) If, for any i, $\Delta_{1i} > 2^{-14} V_{oi}$, the program continues the calculation and the following tests on Q are performed:

   a) $Q < Q_1$ then $h' = \sqrt{2} \cdot h$.

   b) $Q \geq Q_1$ and $Q \leq Q_2$ then $h' = h$.

   c) $Q > Q_2$ then $h' = 0.5\ h$.

There have been 4 test runs made, using one delayed neutron group and no feedback equations with r(t) = \$0.5. The following errors have been found.

Upper Value Q	Lower Value Q	Error	h
10^{-3}	10^{-4}	2.5×10^{-3}	0.0798
10^{-4}	10^{-5}	0.9×10^{-4}	0.014
10^{-5}	10^{-6}	0.6×10^{-5}	0.0035
10^{-6}	10^{-7}	4.0×10^{-6}	0.0017

The above runs were made without feedback terms. For a Q band $\leq 10^{-6}$, 10^{-7} there is a buildup of round-off error. It will also be noted that the error is approximately equal to $\frac{1}{2}(h\omega)^2$.

From the above runs it was calculated that the program computes approximately 10 pt/sec.

III. ANALYSIS OF INHERENT SHUTDOWN MECHANISMS FOR THE KEWB "A" CORE

A. RELATIVE EFFECTIVENESS OF TEMPERATURE AND VOID GROWTH AS FUNCTION OF STABLE PERIOD

The ionization produced by fission fragments slowing down in the KEWB reactor fuel solution (and that from neutrons, beta rays, and gamma rays) results in the formation of approximately 0.2 moles of radiolytic gas ($2H_2 + O_2$) per megajoule of coolant thermal energy released in both the full and underfull core. Depending upon the time scale of the transient as determined by the reactor period, part of the radiolytic gas appears as void volume important in the self-limitation of the burst. Void volume in the core reduces the reactivity mainly by increasing the neutron leakage through density reduction. A given amount of void volume (or temperature increase) produces more reactivity feedback in the full core than in the underfull core, because the reactivity effect of volume change on the core buckling is essentially zero in the full core but is positive in the underfull core

The energy released during operation of the reactor also results in the usual temperature feedback of reactivity In addition to the density and buckling components which are the same for temperature as for gas void, the temperature coefficient of reactivity contains a component which reflects the reduction in nuclear cross-sections with increasing temperature

The reactor stable period range, from periods long enough to approach steady state operation to the shortest which were run with the KEWB "A" core, can be divided into four groups in terms of the relative importance of the shutdown mechanisms. The transition from group to group is gradual in the reactor; numbers assigned to group endpoints are for convenience in discussion

1. Reactor periods from the approach to steady state operation down to 100 sec.

Although the energy released up to the time of peak power in long period transients is substantial, the amount of radiolytic gas formed does not contribute greatly to the reactor shutdown. This is probably because the transient proceeds so slowly that the gas bubbles formed by diffusion have time to escape from the fuel solution. Therefore, there is never a sufficiently large number of bubbles in the fuel solution to

furnish enough void volume to affect the reactivity appreciably. Inherent shutdown of the reactor is accomplished by the negative temperature feedback of reactivity.

2. Reactor periods from 100 sec down to 1 sec.

In this period region, there is more gas present as a result of increased energy release before peak power. Additionally, the time scale of the transient passes through the value of the probable bubble residence time in the fuel solution, so that bubbles will accumulate to contribute significant void volume. Through a large part of this period region, void volume supplies as much or more negative reactivity feedback as temperature in terminating the burst.

3. Reactor Periods from 1 sec down to 30 msec.

In this period region, the time scale of the transient becomes shorter than the time scale for the diffusion of radiolytic gas into bubbles from a moderately supersaturated solution. The transient, therefore, appears to "run away" from the void production mechanism; and the temperature effect again is dominant in turning over the burst. After peak power at the short period end of this region, the burst terminates more rapidly than temperature feedback alone would indicate, heralding the mechanism which becomes important at periods less than 30 msec. The total energy release and that to peak power for this period region and shorter periods, in both the full and underfull core, is shown in Figure 4.

4. Periods less than 30 msec.

In this period region, the KEWB peak power departs materially from the proportionality to the square of the reciprocal period exhibited by reactors which are shut down by prompt temperature effects only, and are described by the well-known Fuchs model of space-independent reactor kinetics equations. The peak power in KEWB is proportional to a decreasing exponent of the reciprocal period (see Figure 5), at periods shorter than prompt critical in the underfull core. This exponent becomes 1.5 in the neighborhood of 2-msec transients. This means that, in addition to the prompt temperature effect, some phenomenon which is becoming more effective as the period is reduced is contributing to the reactor shutdown. Furthermore, inertial pressures appear in the core at about the same period as this shutdown mechanism. Inertial pressure is defined as pressure originating from the solution being driven to expand more rapidly than it can.

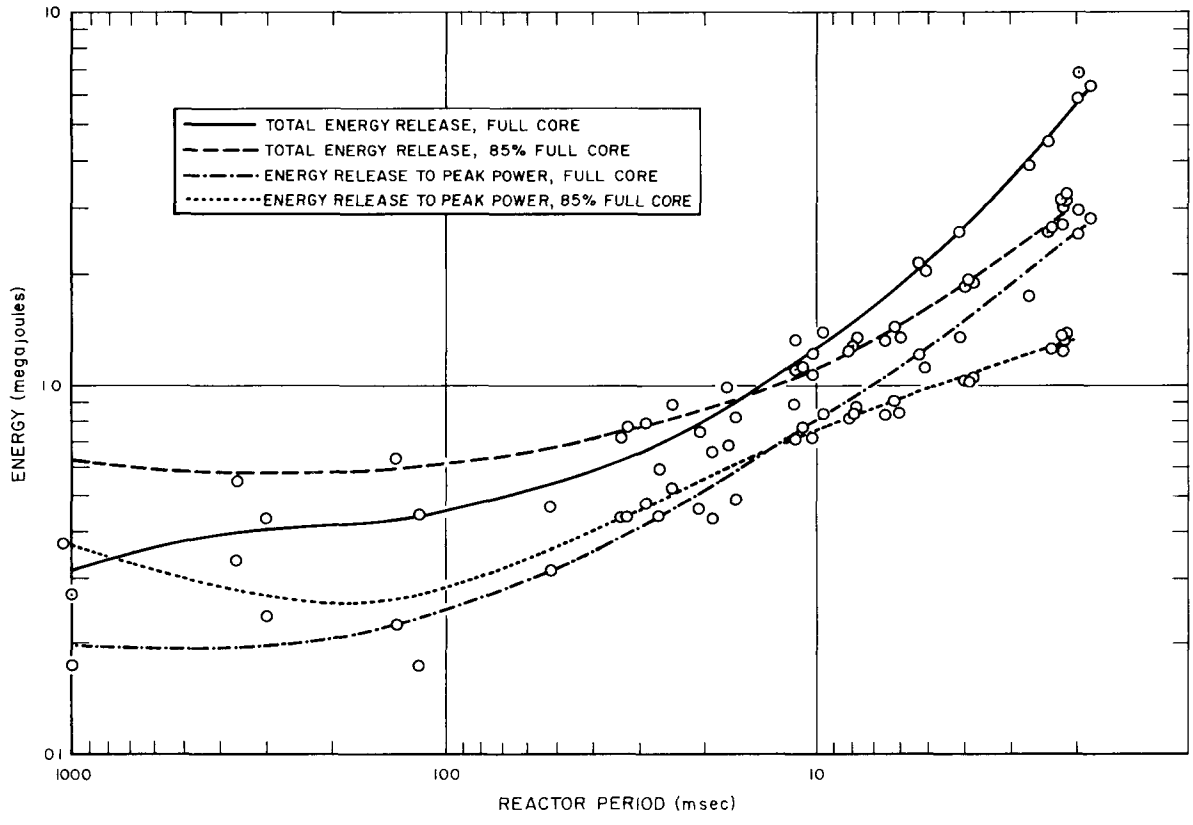

Figure 4. KEWB Spherical Core Energy Release as Function of Reactor Period

The time required for the solution to expand is determined by the speed of sound in the solution and its volume. In order for inertial pressures to appear in the KEWB core at periods in the millisecond or tens of milliseconds range, the speed of sound must be considerably slower than in water containing no gas bubbles[5]. Therefore the appearance of inertial pressures at 20- or 30- msec periods in the KEWB implies that gas bubbles are present in the fuel solution.

That the voids cannot be attributed to steam formation is suggested by the fact that curves of transient pressure as a function of solution temperature are rising much more rapidly than the vapor pressure curve for the solution. For example, in the 2-msec case, the saturation temperature (61°C) which corresponds to the initial pressure of 15 cm Hg was reached slightly after the instant of peak power, but the pressure in the fluid had meanwhile risen to about 10 atm.

Furthermore, the fact that the solution has not expanded sufficiently to fill the sphere completely at the time of peak power, even in the 2-msec case, has two important implications: (1) fuel ejection does not contribute to stopping the

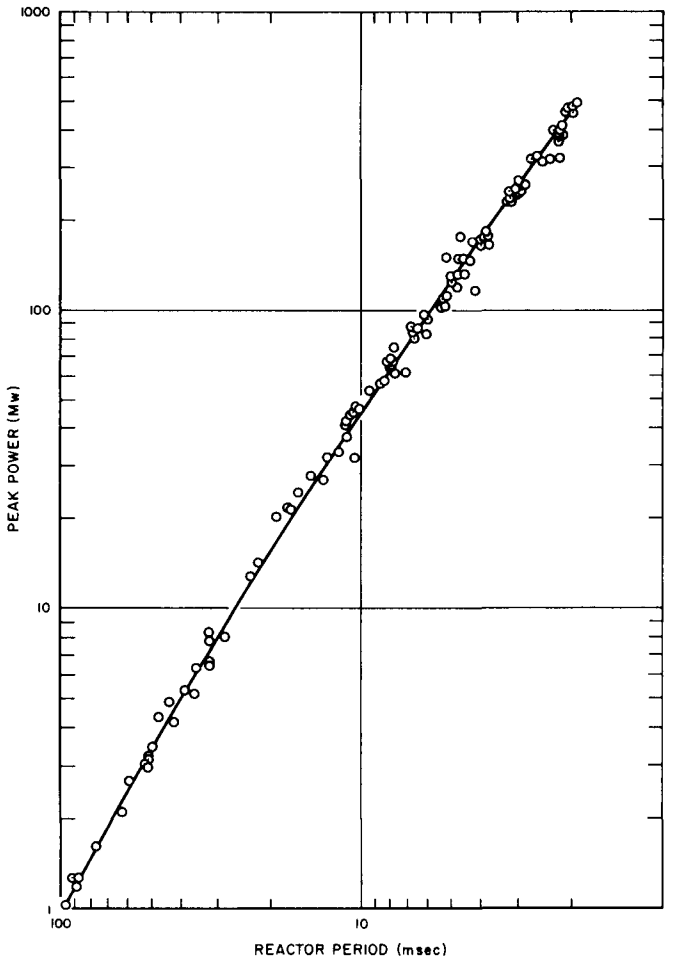

Figure 5. Peak Power as a Function of Reactor Period, Underfull Core

power rise; and (2) the transient pressures which appear for periods shorter than 30 msec are not caused by the constriction through which the solution must pass to enter the overflow chamber.

The compensated reactivity as obtained from AIRCOMP analysis (Section I of this report) is roughly directly proportional to the energy release early in the transient, but begins to increase much more rapidly than the energy a period or two before the peak power. This indicates that the gas void volume is delayed relative to the energy release.

The requirements of increasing effectiveness with decreasing period and delay at peak power relative to an energy proportional phenomenon are met by a reactivity-compensating mechanism which is a higher order function of the energy release.

The status of development of a detailed physical model for the short period radiolytic gas void is discussed in the following section, and one detailed model is presented at length.

B. BUBBLE GROWTH THEORIES

1. General Observations

Computation of the radiolytic gas-compensated reactivity from the integral reactor experiments is complicated by the presence of reflector delayed neutron (Section V) and temperature reactivity feedback effects. Since both of these are subject to uncertainties, the exact amount of radiolytic gas present during short period transients as calculated from the void compensated reactivity is subject to considerable uncertainty. The void volume must be known, however, to determine the merit of proposed models of bubble growth which are necessary to enable prediction of the characteristics of water boiler reactors.

Capsule experiments, in which transient void growth can be measured in the KEWB core environment without the obscuring effects of reflector delayed neutrons or dynamic temperature effects, are in progress in conjunction with the "B" (cylindrical) core experiments. These will ultimately provide sufficiently precise void growth data to permit critical evaluation of void growth models.

Before the effects of reflector delayed neutrons on the reactivity were completely understood, a model of bubble formation and growth at short periods was constructed on the assumption that all the reactivity not compensated by temperature or held in fission product delayed neutrons was provided by gaseous void. Modification of the model to include reflector delayed neutron effects has not been attempted because recent in-pile capsule experiments have shown other areas in which it is deficient. The model is presented here mainly for historical purposes, but also because it contains basic material about void growth in the reactor.

The model is termed the interaction model because it postulates that radiolytic gas-bubbles grow through collisions or near collisions of fission fragment tractks with pre-existing small, hard bubbles.[6]*

A number of theoretical models have been constructed to account for the observed dynamics of bubble growth in KEWB at short periods, for example: (a) diffusion growth in a homogeneous solution; (b) surface nucleation followed by diffusion; (c) coalescence of small bubbles; (d) interaction of active fission tracks; (e) fission track "explosion" followed by diffusion; and (f) charged bubble growth.

* The remainder of this section was edited from the referenced paper by D. P. Gamble.

These models failed for one or more of the following reasons: (a) they predicted, contrary to observation, that the void will decrease as time available for growth decreases; (b) they required lifetimes for transitory physical and chemical reactions far in excess of any plausible value; (c) they required times for bubble growth in excess of that available; (d) they predicted a dynamics of void growth contrary to observation.

The interaction model does not suffer from the above limitations. In it the hypothesis is made that during the interaction a fraction of the radiolytic gas produced in the fission track wake is transferred into the bubble either by surface tension or by diffusion which leads to void growth. The initial bubbles are produced within the wake of a preceding fission fragment. They are believed to be limited to sizes of the order of 10^{-7} cm.

2. Experimental Observations.

The basic characteristics of the void have been determined from experimental data. They will be reviewed briefly.

a) The appearance of inertial pressure in transients commencing with periods around 20 msec is proof that the core contains voids[5].

b) The time available for growth decreases as the rate of void formation and the total amount of void produced increases. This fact is easily demonstrated from a study of void compensated reactivity as a function of period.

c) The void is virtually incompressible for pressure changes of up to 30 atmospheres, which have been produced by the inertial pressure. This fact leads to the conclusion that the void must be present in the form of bubbles with high internal pressure. Small bubbles have the high internal pressures required to be consistent with this observation. This point removes from consideration bubbles with radii larger than 10^{-5} cm, at least until after peak power has been reached.

d) The fact that curves of transient pressure as a function of solution temperature are rising more rapidly than the vapor pressure of the solution is strong evidence that steam is not the shutdown mechanism.

e) The quantity of gas produced during a transient is sufficient to fill small bubbles to a high internal pressure. Radiolytic gas production represents 4% of the energy dissipated in the core.

3. Assumptions

The proposed model is based on the following assumptions:

a) The very small bubbles being considered in this discussion are assumed to have a lifetime greater than 20 msec. These bubbles are subcritical in size. Therefore, according to classical thermodynamics, they should collapse in times much shorter than 20 msec. However, there is a considerable body of experimental evidence in the literature[7,8,9,10] which can be used to support the contention that small bubbles or nuclei can exist for times substantially longer than this.

b) The space-independent reactor kinetics equations can be used with appropriate coefficients to determine system void volume at any time during the transient.[3,11]

c) The average temperature of the gas in the void is assumed to be the same as that of the solution temperatures at the same time.[12]

d) The number of moles of gas, M, available in the system at any time during a transient is the product of the statically determined energy coefficient of gas production, G, and the energy release, E(t).

$$M(t) = GE(t) \qquad \ldots(43)$$

e) It is assumed that the pressure inside the bubble due to surface tension is given by $\frac{2\gamma}{r}$, where γ is the surface tension. In other words, the system hydrostatic pressure, p_∞, is negligible compared to surface tension pressure.

f) Finally, bubbles grow as the result of gas transfer from a fission track to the bubble in fission track bubble collisions.

4. Treatment of an Ensemble of Small Bubbles, to Determine the Average Bubble Radius

An ensemble of bubbles may be described in terms of several different weighted averages of bubble radius. The most useful average is one weighted by the number of moles of gas in each radius interval.

Consider an ensemble of gas bubbles where the number of bubbles with radius between r and r + dr is $\xi(r)$. Assume for the moment that the bubble-size distribution function $\xi(r)$ is known, and is a continuous function of bubble radius in the interval from the smallest bubble radius, r_o, which contains just one gas molecule per bubble up to a maximum radius bubble, r_{max}, for the ensemble.

The number of moles of gas, n, contained in any one bubble of radius r is:

$$n = \frac{pV}{R_g T} = \frac{\frac{2\gamma}{r} \cdot \frac{4}{3}\pi r^3}{R_g T} = \frac{8\gamma\pi r^2}{3R_g T} \qquad \ldots(44)$$

where R_g is the gas constant per mole, and T the absolute temperature. The total number of moles of gas contained in $\xi(r)\,dr$ bubbles of size r is

$$dM = \frac{8\gamma\pi}{3R_g T} \cdot \xi(r)dr, \qquad \ldots(45)$$

and the total moles of gas in the bubble ensemble is

$$M = \frac{8\gamma\pi}{3R_g T} \int_{r_o}^{r_{max}} r^2 \xi(r)dr. \qquad \ldots(46)$$

The mole-weighted average bubble radius is

$$\bar{r}_{mole} = \frac{\int r dM}{\int dM} = \frac{\frac{2\gamma}{R_g T}\int_{r_o}^{r_{max}} \frac{4\pi r^3}{3}\xi(r)dr}{\int_{r_o}^{r_{max}} \frac{8\gamma\pi r^2}{3R_g T}\xi(r)dr} . \qquad \ldots(47)$$

The denominator of Equation 47 is easily identified as the total number of moles of gas in the bubbles which make up the ensemble, M. By rearrangement of the numerator as indicated in Equation 47, one is able to recognize the integral as the sum of the volume of each bubble making up the ensemble or the total volume occupied by bubbles V_B. Hence, Equation 47 becomes

$$\bar{r}_{mole} = \frac{2\gamma V_B}{MR_g T} , \qquad \ldots(48)$$

And by defining an effective bubble pressure p_B as equal to $\frac{2\gamma}{\bar{r}_{mole}}$, then Equation 48 becomes

$$p_B = \frac{MR_g T}{V_B} ,$$

which has the same form as the perfect gas law. The similarity in form between Equation 49 and the perfect gas law suggests that the behavior of the ensenble under compression may be treated by using p_B and V_B in Boyle's law. Detailed examination of this question has shown that the ensemble never exactly follows the Boyle's law relation. However, numerical investigation, assuming different bubble size distributions, has suggested that the errors introduced by using Boyle's law are relatively small (<10%). Unless bubble-size distribution anomalies exist in the fuel solution which renders the deduction based on these numerical computations greatly in error, one can say that $\frac{1}{p_B}$ is a good measure of the compressibility $\left[\frac{1}{V}\left(\frac{\partial V}{\partial p}\right)_t\right]$ of the bubble ensemble.

The value of the mole-weighted average bubble radius is readily computed from the experimental data. The volume occupied by the bubbles is obtained from the void compensated component of the reactivity and the void coefficient of reactivity. The number of moles of gas produced is simply the energy released times the static gas production coefficient. The value of $\bar{r}_{mole}$ can be computed at any time during the transient without knowledge of $\xi(r)$.

In Figure 6, the value of $\bar{r}_{mole}$ at the time of peak power is plotted vs reactor period for a group of KEWB transients. In the period range from 20.0 to 0.1 sec, the energy release up to the time of peak power varies by less than ± 10% of the average value. However, in the same period range the average bubble size at peak power decreases rapidly as the period decreases. Gas filled voids are ineffective as as a shutdown mechanism in this region because the gas is contained under high pressure, that is, small volume. As the period becomes shorter than 0.1 sec the bubble size increases from about 10^{-6} to 10^{-5} cm. Hence, the internal pressure of the gas in the bubbles will be between 140 and 14 atmospheres. Fuel solution containing bubbles will have a much larger compressibility than that of the bubble-free solution; however, as

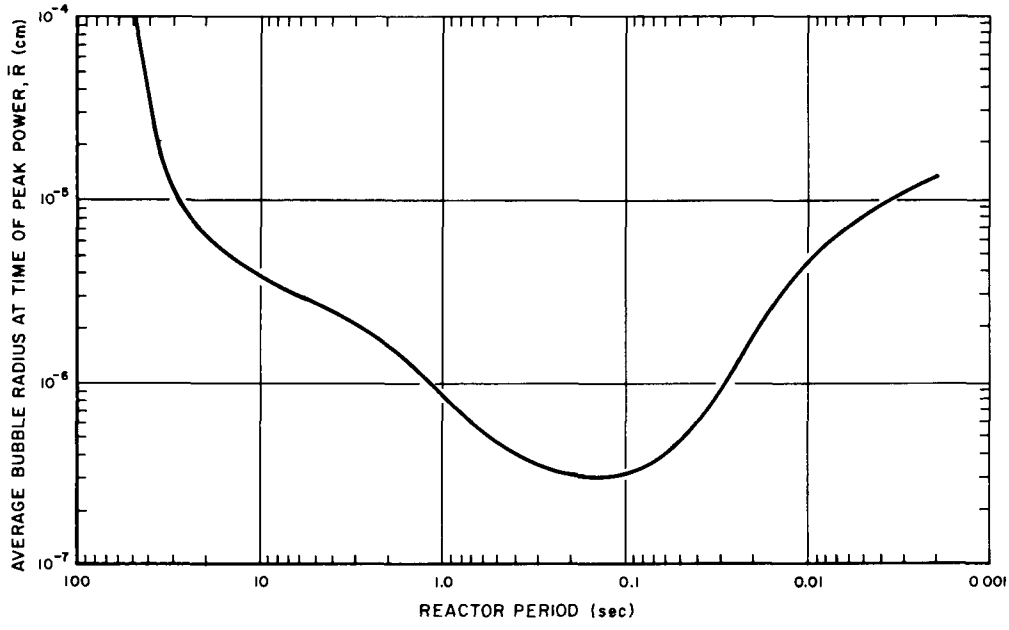

Figure 6. Average Bubble Radius at Time of Peak Power as a Function of Reactor Period

required by experiment, the compressibility is still small enough so that the inertial pressure has relatively little effect on total void volume.

The change in mole-average bubble radius as a function of time during the power excursion is shown for a fast transient (τ = 3.74 msec) in Figure 7.

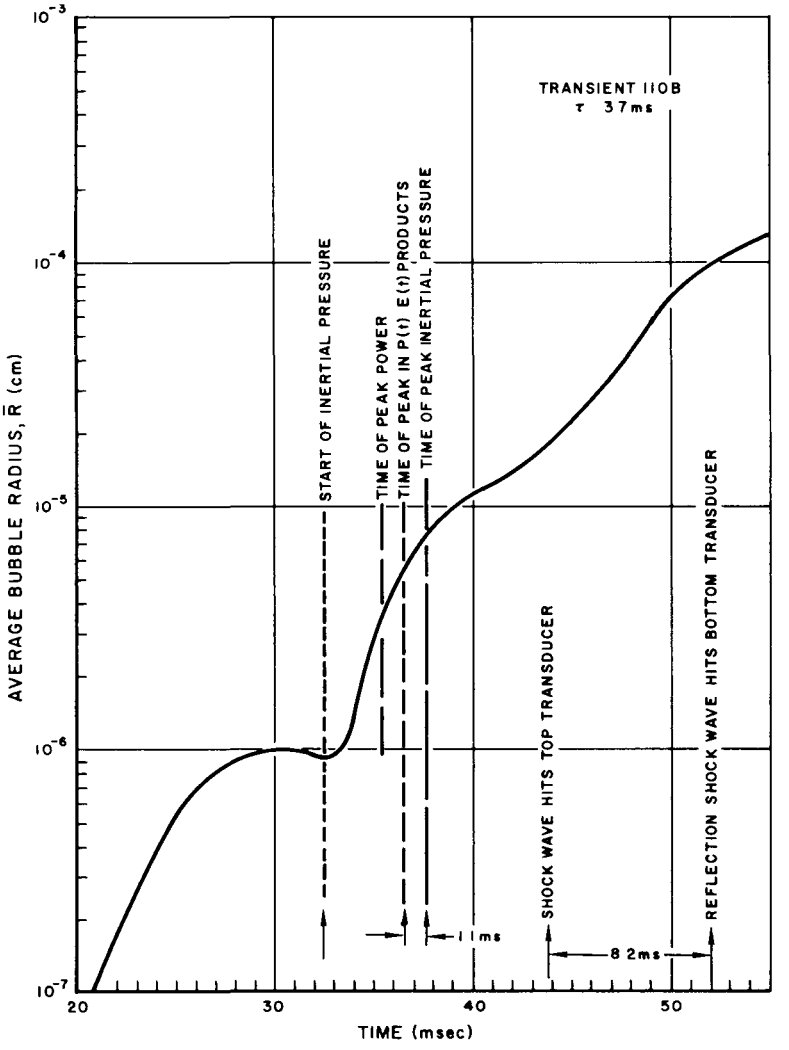

Figure 7. Average Bubble Radius as a Function of Time

The validity of the mole-average bubble radius has been checked by comparing the time it takes sound to traverse the core with that computed using the bubble radius of Figure 7 and the volume fraction of gas present in the core[13]. The comparison is made in the following way.

It will be shown later that, from both experimental and theoretical considerations, the rate of void production is proportional to the product of power and energy; that is, proportional to N · E (see Equation 60). Void-formation is the driving force for the production of inertial pressure. Hence, the time lag between the peak of the driving function and the observed peak in the inertial

pressure is a measure of the time required for sound to cross the fuel solution. This time lag from the experimental data is about 1.1 msec corresponding to a speed of sound of 196 m/sec. The value computed from bubble size and volume is 200 m/sec, which is in excellent agreement. While this agreement may be somewhat fortuitous, it does indicate that Equation 48 is a good description of the void.

Later in the transient (shown in Figure 7), in the time region between 43.8 and 52 msec, a shock wave which was formed by the constricting effects at the top of the core required 8.2 msec to reach the bottom of the core. This corresponds to sound velocities of 38 m/sec. A bubble size of about 5×10^{-5} cm would yield this velocity of sound when the original core solution just filled the sphere, giving a 15% void volume. The average bubble radius computed from Equation 48 in this time interval is about 4×10^{-5} cm, again in excellent agreement.

5. Interaction Model of Bubble Growth

In the preceding section we have shown that a meaningful physical description of the void is possible in terms of an average bubble radius computed by Equation 48. We therefore are now in a position to investigate quantitatively the concept that collisions between fission tracks and bubbles result in the bubble-growth phenomenon observed in the KEWB reactor.

The number of collisions per unit time between a fission fragment and a bubble will be the product of the fission fragment flux times the microscopic bubble cross-section. The average fission fragment production rate per unit volume in the core is $2 \times 3.1 \times 10^{16} \bar{N} V_{core}^{-1}$, $\bar{N}$ in megawatts. The removal rate of fragments is $f\bar{t}^{-1}$, where f is the fragment density, and $\bar{t}$ the average time in which the fragment is traversing its track. Therefore,

$$\frac{df}{dt} = \frac{6.2 \times 10^{16}}{V_{core}} \bar{N}(t) - \frac{f}{\bar{t}} \qquad \ldots(50)$$

Since $\bar{t}$ is many orders of magnitude shorter than the time scale upon which the power is changing, $df/d\bar{t} \sim 0$, so that

$$f = \frac{6.2 \times 10^{16} \bar{N}(t) \bar{t}}{V_{core}} \quad . \qquad \ldots(51)$$

And since $\bar{t} = \bar{L}\bar{v}$, where $\bar{L}$ is the average distance travelled by the ionizing fragment and $\bar{v}$ its average velocity, the fission fragment flux is

$$\bar{\phi}_F(t) = f\bar{v} = \frac{6.2 \times 10^{16} \bar{L}\bar{N}(t)}{V_{core}} \qquad \ldots(52)$$

The microscopic bubble cross-section is defined as the geometrical projected area of the bubble, πr^2. The number of collisions per bubble in a second is the fission fragment flux times the microscopic cross-section. Hence, it is apparent that the large bubble will have a much higher probability of collision than will a small bubble. If each collision leads to bubble growth, then the chance of future interactions increases rapidly with each collision.

The macroscopic bubble cross-section, Σ_B, is the sum of the microscopic cross-sections of each bubble present in a cubic centimeter of fuel solution. The number of bubbles per unit volume of the solution is

$$\text{No. of bubbles} = \frac{1}{V_{core}} \int_{r_o}^{r_{max}} \xi(r)dr, \qquad \ldots(53)$$

Therefore

$$\Sigma_B(t) = \int_o^{r_{max}} \frac{\pi r^2}{V_{core}} \cdot \xi(r)dr. \qquad \ldots(54)$$

And, with recourse to Equations 46 and 43, Equation 52 becomes

$$\Sigma_B(t) = \frac{3R_g TG}{8\gamma V_{core}} \cdot E(t). \qquad \ldots(55)$$

The resulting macroscopic cross-section is independent of bubble size, or the bubble size distribution function. Since the lower limits of the integration included bubbles with just one molecule of gas per bubble, no distinction need be made between dissolved gas and gas contained within larger bubbles. It is clear that the void volume and gas volume are not identical. In particular, a one-molecule bubble will not contribute to the void. However, as a result of the r^2 in the averaging processes discussed earlier, this distinction leads to small departures from the description given by Equation 48. The number of collisions between bubbles and fission fragments is then

$$C_{F \rightarrow B}(t) = \Sigma_B(t) \cdot \phi_F(t) = \frac{\text{Collisions}}{\text{cm}^3\text{-sec}}. \qquad \ldots(56)$$

Substituting Equations 50 and 53 into 54 gives

$$C_{F \rightarrow B}(t) = \frac{3 \times 6.2 \times 10^{16} R_g T G \bar{L}}{8 \; V^2_{core}} \cdot N(t) \cdot E(t). \qquad \ldots(57)$$

Letting ϵ be equal to the constant and approximately constant terms, Equation 57 becomes

$$C_{F \rightarrow B}(t) = \epsilon \cdot N(t) \cdot E(t) . \qquad \ldots(58)$$

The value of ϵ is

$$\epsilon = 3.3 \times 10^{14} \frac{\text{Collisions}}{\text{cm}^3(\text{Mw-sec})^2} \qquad \ldots(59)$$

It is most interesting to note that the number of collisions per unit time is dependent only on the product of power and energy. The analysis of the experimental data shows that the void volume also appears to depend only on the product of power and energy;[3,11] that is,

$$\frac{dV}{dt} = \nu N(t) \cdot E(t) \qquad \ldots(60)$$

or

$$V = \frac{1}{2}\nu E(t)^2 \quad . \qquad \ldots(61)$$

The value of ν determined from the experimental data is $500 \frac{Cm^3}{(Mw\text{-}sec)^2}$.

If a volume of gas transferred into the bubble per collision is a constant amount K per collision, then the rate of void growth will be

$$\frac{dV}{dt} = K \cdot V_{core} C_{F \rightarrow B}(t) \quad . \qquad \ldots(62)$$

The number of collisions per second per unit volume must be multiplied by the core volume V_{core} to obtain the total rate of void growth. Returning to Equation 58 for the number of collisions, Equation 62 becomes

$$\frac{dV}{dt} = K\epsilon V_{core} N(t) \cdot E(t) \qquad \ldots(63)$$

where K, ϵ and V_{core} are constant. The form of Equation 63 is now identical to the experimentally determined empirical Equation 60. Therefore, the constant terms can be equated so that

$$\nu = K\epsilon V_{core} \qquad \ldots(64)$$

and the value of K can be determined as $1.9 \times 10^{-16} cm^3/collision$.

An alternate assumption to the constant volume increment per collision is the concept that a constant number of moles are transferred on the average per collision. Consider one bubble, then let a constant average number of moles of gas, $\bar{n}$, be deposited in the bubble per collision. Then, the radius r_i of the bubble after the i^{th} collision will be

$$r_i = \left[\frac{3R_g T}{8\gamma\pi}(\bar{n} \cdot i + n_o)\right]^{-1/2} \qquad \ldots(65)$$

where n_o is the number of moles of gas in the original bubble. The initial bubbles produced without interaction in the fission track wake are believed to have a radius comparable to the radius of the intensely ionized region of the track, which is probably about 50Å. A bubble 50Å in radius contains 3.4×10^2 molecules of gas. From the static gas production coefficient, one can compute that 1.7×10^6 gas molecules are produced in each fission-track wake. If only 1.0% of the gas in the track were transferred to a bubble per collision, then it is clear that the number of moles of gas in the bubble would be negligible. Therefore, n_o in Equation 65 is negligible, and the volume of the bubble V_i after the i^{th} collision is

$$V_i = \frac{4\pi}{3} r_i^3 = \frac{4\pi}{3}\left(\frac{3R_g T}{8\pi\gamma}\right)^{3/2} (\bar{n} \cdot i)^{3/2} . \qquad \ldots(66)$$

The next step is to compute the microscopic cross-section for the non-collided, 1st, 2nd, ... collided bubble groups. This computation requires a knowledge of the bubble size distribution function $\xi(r)$ as a function of time during a transient. No attempt has been made to solve this problem. However, progress can be made in a more restricted case where it is assumed that only one collision per bubble can occur. Under this restriction, i = 1 and Equation 66 becomes

$$V_{i=1} = \frac{4\pi}{3}\left(\frac{3R_o T}{8\gamma\pi}\right)^{3/2} \bar{n}^{3/2} . \qquad \ldots(67)$$

All of the terms in the right hand side of Equation 67 are constant, therefore $V_{i=1}$ is constant and is equal to the volume of gas transferred per collision, but this is equal to K in Equation 62. Therefore, the assumption of only one hit per bubble converts the constant-mass-transferred-per-collision model into the constant-volume-transferred-per-collision model. Setting Equation 67 equal to the value of K (1.9×10^{-16} cm^3/collision), and solving for $\bar{n}$, we obtain 3.0×10^{-19} moles, or 1.8×10^5 moles per collision. The value of $\bar{n}$ is, therefore, a factor of 1000 larger than n_o. This shows the assumption to be valid that n_o can be neglected.

The number of molecules transferred is about 10% of the gas available along the fission-fragment track. Therefore, it is apparent that more than sufficient radiolytic gas is available in the track, and that the number of collisions are adequate to explain the KEWB reactor bubble growth.

The more general computation of void growth assuming multiple collisions with constant mass transfer will resemble the constant-volume computation in the early stages of the transient. In this time region of the transient, relatively few singly collided bubbles will be present compared to the noncollided bubbles. As the transient proceeds, however, the inventory of once hit bubbles will increase, so that multiple collisions will become important. When this happens, the void growth will be faster than that given by the power and energy product model. The difference between the two models could be expressed in terms of some appropriately averaged $(\bar{i})^{3/2}$. The value of i may be relatively unimportant until after peak power in the very fast transients.

IV. DEVELOPMENT OF MATHEMATICAL MODEL OF REACTOR

As was the case for the model of void growth at short periods described in the preceding section, the partial solutions to the reactor kinetics equations with feedback from void growing at a rate proportional to the product of power and energy were derived without incorporation of reflector delayed neutron effects. The presence of reflector-delayed neutrons invalidates the assumption made below that delayed neutron feedback can be neglected at periods shorter than 30 msec. For reflector materials with an appreciably shorter thermal diffusion time than graphite, however, or for bare core operation, the following analysis will be applicable if there is prompt temperature plus a second reactivity feedback mechanism which grows at a rate proportional to the product of power and energy. Such a reactor can be described by the space-independent system of equations:

$$\frac{dN}{dt} = \frac{\beta}{\ell}\left[(R - 1)N + \sum_{i=1}^{6} f_i W_i\right] \qquad \ldots(68)$$

$$\frac{dW_i}{dt} = \lambda_i (N - W_i), \qquad i = 1, \ldots, 6 \qquad \ldots(69)$$

$$\frac{dT}{dt} = KN - \gamma T \qquad \ldots(70)$$

$$\frac{dV}{dt} = VN(t)\int_o^t N(x)dx - \sigma V \qquad \ldots(71)$$

$$N = \frac{dE}{dt} \qquad \ldots(72)$$

$$R = R_o(t) + \alpha T + \phi V \qquad \ldots(73)$$

where the symbols employed in the first two equations have been defined in section IB, and

T = temperature rise,

K = reciprocal heat capacity,

γ = reciprocal heat transfer characteristic time,

V = void volume,

ν = adjustable parameter,

σ = reciprocal of bubble residence time,

E = energy release,

α = temperature coefficient of reactivity

and ϕ = void volume coefficient of reactivity

The temperature and void volume coefficients of reactivity are both negative for aqueous homogeneous reactors. The term γT in the temperature rise equation is a simple correction for heat loss. The analogous term in the void volume equation, σV, has been included to represent bubble collapse or escape from the solution. The proportionality of the rate of void-volume growth to the product of power and energy release in this equation can be viewed as a phenomenological model for the reactor behavior without reference to the details of void formation.

General analytic solutions to the kinetics equations cannot be obtained, but computer solutions are available in the AIREK program discussed in Section I. C. These have been employed extensively for comparison with the experimental burst shape, and for parameter studies to determine the sensitivity of the KEWB performance to variations in the system constants. In the latter capacity, computer runs fall short of providing the insight obtainable from analytic relationships. The deficiency is filled with the following partial analytic solutions to the kinetics equations.

For periods of 30 msec or less, the delayed neutrons can be neglected until some time after peak power. Also, γ and σ are negligible in this period range. Therefore the kinetic behavior of the reactor under the stated conditions can be described by the simplified set of equations:

$$\frac{dN}{dt} = \frac{\beta}{\ell}(R - 1)N \qquad \ldots(74)$$

$$\frac{dT}{dt} = KN \qquad \ldots(75)$$

$$\frac{dV}{dt} = \nu NE \qquad \ldots(76)$$

and Equations 72 and 73. Substituting Equation 72 in 75 gives

$$\frac{dT}{dt} = K\frac{dE}{dt} \qquad \ldots(77)$$

or

$$dT = KE \qquad \ldots(78)$$

which, under the condition that T = 0 when E = 0, integrates to

$$T = KE \qquad \ldots(79)$$

Substituting Equation 72 into 76 gives

$$\frac{dV}{dt} = \nu E\frac{dE}{dt} \qquad \ldots(80)$$

or

$$dV = \nu E dE, \qquad \ldots(81)$$

which, under the condition that V = 0 when E = 0, integrates to

$$V = \nu E^2/2 \ . \qquad \ldots(82)$$

Substituting Equations 79 and 82 into 73 gives

$$R = R_o(t) + \alpha KE + \phi\nu E^2/2 \ . \qquad \ldots(83)$$

Note that the term derived from the void is just the next term in an energy polynominal feedback of reactivity. This would be expected to provide a better fit if the temperature feedback only were not adequate, regardless of the physical applicability of the term ascribed to void. Letting $\alpha K = \epsilon_1$ and $\phi\nu = \epsilon_2$ we can now substitute Equation 83 for the reactivity in 74, which gives, using 72,

$$\frac{dN}{dt} = \frac{\beta}{\ell}\left[R_o(t) + \epsilon_1 E + \epsilon_2 \frac{E^2}{2} - 1\right]\frac{dE}{dt} . \qquad \ldots(84)$$

By limiting the reactivity input to steps, $R_o(t) = R_o(\text{constant})$, this becomes

$$dN = \frac{\beta}{\ell}\left[R_o + \epsilon_1 E + \epsilon_2 \frac{E^2}{2}\right]dE \qquad \ldots(85)$$

which can be integrated directly, and with the condition that N = 0 when E = 0 gives

$$N = \frac{\beta}{\ell}\left[(R_o - 1)E + \epsilon_1 \frac{E^2}{2} + \epsilon_2 \frac{E^3}{6}\right]; \qquad \ldots(86)$$

or, using the relation

$$\frac{\beta}{\ell}(R_o - 1) = \omega_o , \qquad \ldots(87)$$

which is the asymptotic form of the inhour equation for short period transients, this becomes

$$N = \omega_o E + \frac{\beta}{2\ell}\left[\epsilon_1 E^2 + \frac{E^3}{3}\right]. \qquad \ldots(88)$$

Before proceeding with the useful relations which can be derived from Equations 85 and 88, one further integration of 88 can be made. Using Equation 72, and defining $L = \ell/\beta$, Equation 88 can be written

$$\frac{dE}{dt} = \frac{E}{2L}\left(2\omega_o L + \epsilon_1 E + \epsilon_2 \frac{E^2}{3}\right) \qquad \ldots(89)$$

$$\frac{\beta}{2\ell}dt = \frac{dE}{E\left(2\omega_o L + \epsilon_1 E + \epsilon_2 E^2\right)} . \qquad \ldots(90)$$

This relation can be integrated to give

$$2\omega_o t = \ell n \frac{6E^2}{6\omega_o L + 3\epsilon_1 E + \epsilon_2 E^2}$$

$$- \left(1 - \frac{8\epsilon_2 \omega_o L}{3\epsilon_1^2}\right)^{-1/2} \ell n \frac{2\epsilon_2 E + 3\epsilon_1 - 3\epsilon_1 \sqrt{1 - 8\epsilon_2 \omega_o L/3\epsilon_1^2}}{2\epsilon_2 E + 3\epsilon_1 + 3\epsilon_1 \sqrt{1 - 8\epsilon_2 \omega_o L/3\epsilon_1^2}} \quad \ldots(91)$$

Unfortunately, this cannot be solved explicitly for E as a function of t, which relationship could then be differentiated to give an equation for the burst shape, valid for step reactivity inputs to shortly after peak power. However, from Equation 91 we can use E as our independent variable and find t = t(E). From Equation 89 we have

$$N = \frac{dE}{dt} = N(E) \quad \ldots(92)$$

and hence we can plot N as a function of t in parametric form.

Approximations to E as a function of t can be found for E small and E large. Further manipulation of the above equation remains an item for future effort.

Since dN/dt = 0 at peak power, the expression in parenthesis on the right-hand side of Equation 85 must be equal to zero; that is, using notation $\hat{E}$ for energy release to the power peak,

$$R_o - 1 + \epsilon_1 \hat{E} + \epsilon_2 \hat{E}^2/2 = 0 ; \quad \ldots(93)$$

or, using Equation 87,

$$\omega_o \frac{\ell}{\beta} + \epsilon_1 \hat{E} + \epsilon_2 \hat{E}^2/2 = 0 . \quad \ldots(94)$$

Solving this quadratic for $\hat{E}$ gives

$$\hat{E} = \frac{-\epsilon_1 \pm \sqrt{\epsilon_1^2 - 2\epsilon_2 \omega_o \ell/\beta}}{\epsilon_2} \qquad \ldots(95)$$

which, upon discarding the negative solution and rearranging, becomes

$$\hat{E} = \frac{\epsilon_1}{\epsilon_2}\left[-1 + \sqrt{1 - \frac{2\epsilon_2 \omega_o \ell}{\epsilon_1^2 \beta}}\right]. \qquad \ldots(96)$$

For the peak power, designated by $\hat{N}$, Equation 94 can be substituted in 88. Note that the form of Equation 94 is such that it can be solved for ω_o, or $\epsilon_1 E$ or $\epsilon_2 E^2$, all of which appear in Equation 88 if E is factored out. Therefore, any one of the three quantities can be eliminated, giving the following three equivalent expressions $\hat{N}$.

$$\hat{N} = \frac{\beta}{\ell}\hat{E}\left(-\frac{\epsilon_1}{2}\hat{E} - \frac{\epsilon_2}{3}\hat{E}^2\right) \qquad \ldots(97)$$

$$\hat{N} = \frac{\omega_o \hat{E}}{2} - \frac{\beta\epsilon_2}{2\ell}\hat{E}^3 \qquad \ldots(98)$$

$$\hat{N} = \frac{2}{3}\omega_o \hat{E} + \frac{\beta\epsilon_1}{6\ell}\hat{E}^2 \qquad \ldots(99)$$

The last of these is most convenient to use as it does not contain $\hat{E}^3$. Equ Equation 96 could be substituted into 99 to give $\hat{N}$ in terms of the system parameters directly, but the resultant expression is complicated. In use, the simplest procedure is to solve for $\hat{E}$ with Equation 96, and substitute the value in 99.

For very short period transients, a great simplification can be made in the equations for energy release to peak power and peak power. This occurs when the amount of temperature compensated reactivity becomes negligible compared

to the amount compensated by void volume, and the terms involving ϵ_1 in the derivations can be omitted. Thus Equations 88 and 94 become respectively,

$$N = \omega_o E + \frac{\beta \epsilon_2}{6\ell} E^3 , \text{ and} \qquad \ldots(100)$$

$$\omega_o + \frac{\beta \epsilon_2}{2\ell} \hat{E}^2 = 0 . \qquad \ldots(101)$$

Solving Equation 101 for $\hat{E}$ gives

$$\hat{E} = \sqrt{\frac{-2\ell\omega_o}{\beta\epsilon_2}} ; \qquad \ldots(102)$$

and substituting this in Equation 100 gives

$$\hat{N} = \frac{2}{3}\sqrt{-2\ell/\epsilon_2\beta}\ \ \omega_o^{3/2} , \qquad \ldots(103)$$

The simplicity of the last two equations reduces parameter studies in the period regions where the equations are valid to a matter of inspection. Some caution is necessary lest the coupling between R, β, ℓ, and ω given by the inhour Equation 87 be overlooked. For example, if it were desired to design a water boiler for maximum flux, Equation 103 indicates that the peak flux will increase in proportion to the square root of increase in the neutron lifetime, all other factors remaining constant. The inhour equation shows that increase in ℓ requires almost proportional increase in the input reactivity to maintain a given value of ω. Additional excess reactivity is difficult and expensive to design into the reactor, however, aside from the fact that increase in the core loading tends to decrease the neutron lifetime. Considering both Equations 87 and 103, it turns out that decreasing ℓ enables attainment of shorter periods with a given maximum excess reactivity, thus maximizing the flux which is more sensitive to the changes in the period than any other parameter.

V. DISCUSSION OF REFLECTOR-DELAYED NEUTRONS

A. EXPERIMENTAL EVIDENCE OF A SHORT-PERIOD ANOMALY

Three independent areas of the KEWB data are not consistent with an analytic representation of the reactor based upon the space-independent kinetics equations containing the conventional six groups of delayed neutrons and temperature and void feedback of reactivity proportional to energy and the product of power and en energy, respectively. These are as follows.

1. The Burst-Shape

A definite change in the burst symmetry occurs as the reactor period approaches 2 msec. Figure 8 shows transients for periods of 9.7, 5.7, 3.7 and

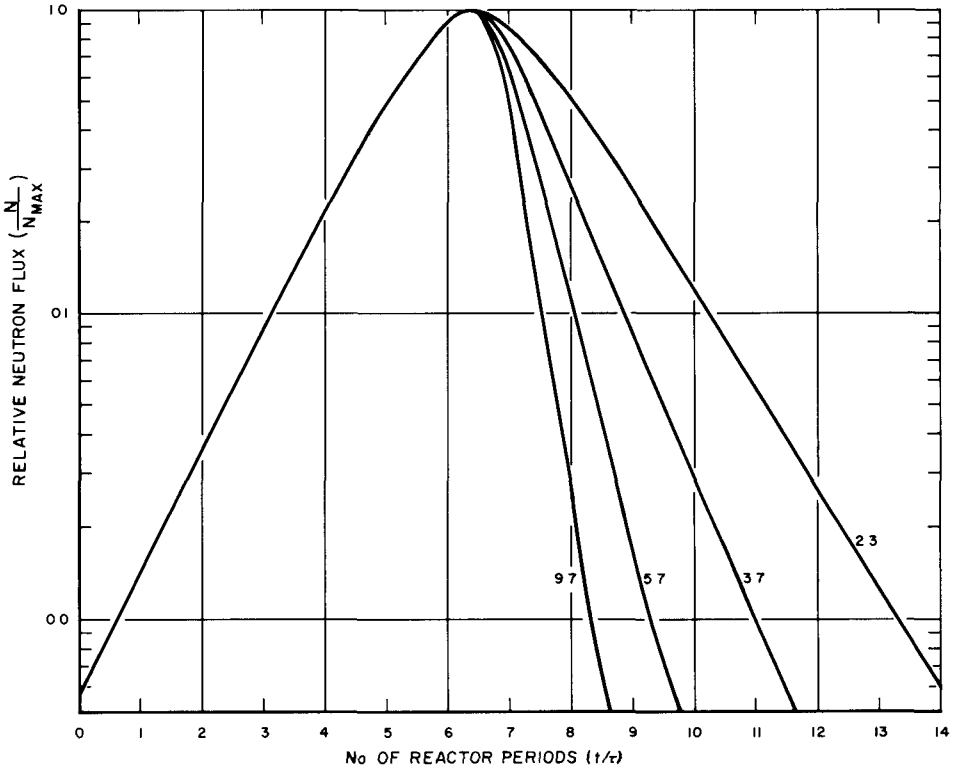

Figure 8. Relative Burst Shape for Periods Shorter than 10 msec, Underfull Core

2.3 msec normalized to unity peak power and number of periods along the time axis. Here we see some process holding the power up after the peak as the period approaches 2 msec.

Holdup of the power after the peak does not agree with the behavior of the shutdown mechanisms, which are becoming more effective as the period is decreased. The latter is illustrated by the slope of the peak power as a function of period curve (Figure 5), which is decreasing with period. Reactivity computations with AIRCOMP also show that the compensated reactivity before peak power is rising more rapidly than the energy release as a function of decreasing period. The holdup of power after the peak must therefore be the effect of some process omitted from the mathematical model.

2. The Pile Oscillator Data

Another manifestation of the anomaly at shorter periods is evidenced in the pile oscillator data.[14] The results of this experiment at high frequencies do not agree with the predictions of the theoretical transfer function. Since the void and temperature reactivity feedback functions become negligible in the transfer function at high frequencies, this experiment indicates that the omission from the mathematical model is a neutronic process.

3. The Experimental Inhour Equation

The third and most inportant departure of data from that expected is found in the experimental inhour curve at periods less than 10 msec. This curve is a plot of step reactivity input to the reactor as a function of the observed stable period. The input reactivity involved in a transient is obtained from the initial critical and final control rod elevations through the control rod calibration curve. Figure 9 shows the inhour curves for the KEWB full and underfull spherical cores, as well as the theoretical inhour curve for six groups of delayed neutrons. The linear plot is employed to emphasize the short period region.

The general form of the inhour equation is

$$\rho = \frac{\ell \omega}{k_{eff}} + \sum_{i=1}^{n} \frac{\beta_i \omega}{\omega + \lambda_i} \qquad \ldots(104)$$

where ρ is the reactivity, ℓ is the apparent neutron lifetime, ω is the reciprocal of the stable period, β_i are the delayed neutron criticality factors, k_{eff} is the effective multiplication factor, and λ_i are the delayed constants. To simplify

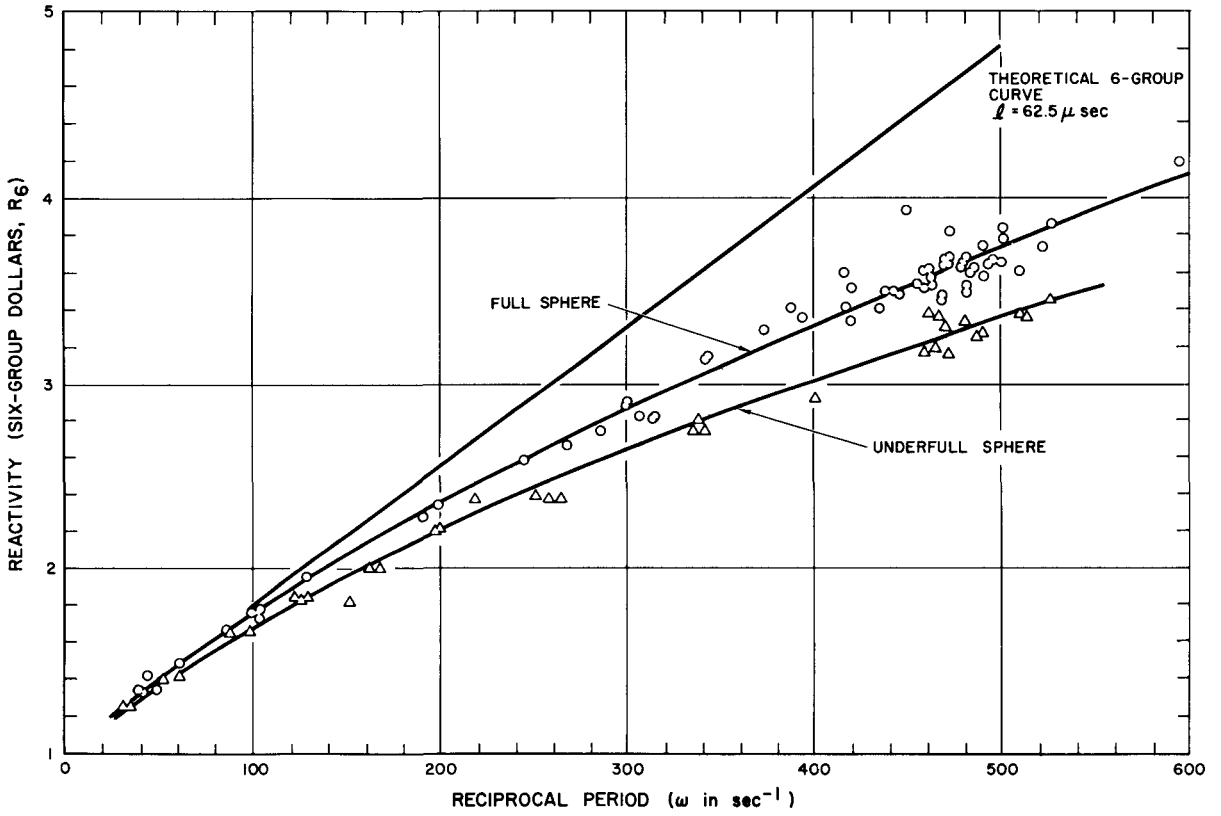

Figure 9. KEWB Spherical Core Inhour Curves

the equation, the effective multiplication is taken to be unity even at short periods The core lifetime increases with k_{eff}, and little error results from this assumption.

Equation 104 is then written

$$\rho = \ell\omega + \sum_{i=1}^{n} \beta_i \sum_{i=1}^{n} \frac{f_i \omega}{\omega + \lambda_i} \qquad \ldots(105)$$

where $f_i = \beta_i / \sum_{i=1}^{n} \beta_i$.

Since the definition of reactivity in dollars is

$$R = \frac{k_{ex}}{\sum_{i=1}^{n} \beta_i} = \frac{\rho k_{eff}}{\sum_{i=1}^{n} \beta_i} \qquad \ldots(106)$$

and k_{eff} has been taken to be unity,

$$R = \frac{\ell\omega}{\beta_{eff}} + \sum_{i=1}^{n} \frac{f_i \omega}{\omega + \lambda_i} \qquad \ldots(107)$$

where $\beta_{eff} = \sum_{i=1}^{n} \beta_i$.

Using the relative delayed neutron fractions for six delay groups of Keepin, Wimett and Zeigler,[15] the KEWB reactor experimental inhour curve can be fitted with Equation 107 down to about $\omega = 100$ sec^{-1} with $\ell/\beta_{eff} = 7.8 \times 10^{-3}$ sec. If $\beta_{eff} = 0.008$, then $\ell = 62.5$ μsec. The extension of the theoretical curve to the short period region with these numbers is that shown in Figure 9.

Substracting 1 from the reactivity figures given by the theoretical and underfull spherical core curves at $\omega = 500$ sec^{-1} gives 3.8 and 2.4 dollars respectively. This means that the value of ℓ/β_{eff} would have to decrease over 50% from $\omega = 100$ to $\omega = 500$ sec^{-1} (10 to 2 msec periods) in order to describe the data with Equation 107. This is unreasonable for either quantity. Therefore, the theoratical inhour equation employed is not an accurate representation of the KEWB reactor for periods less than 10 msec.

B. POSTULATION OF PRESENCE OF REFLECTOR-DELAYED NEUTRONS

The unexpected behavior of the KEWB reactor can be described by addition of a group of delayed neutrons with a relatively large abundance and mean delay time in the millisecond region. Such neutrons would tend to hold up the power after the peak when the reactor period approached their mean delay time. They would also have an effect on the pile oscillator transfer function at high frequencies; and, most definitely, they would influence the form of the inhour curve in the millisecond period region.

If the concept of the presence of a seventh group of delayed neutrons in the KEWB assembly is entertained, it is natural to consider the possibilities of a source of such neutrons. A group with large abundance and mean delay time in the millisecond range could not originate from fission product precursors, for they would have been evidenced in the Godiva reactor experiments.[16] It is hypothesized that these neutrons originate in the KEWB reactor graphite reflector as the fraction of fast neutron leakage which is thermalized and finds its way

back to the core. That such neutrons might well evidence the characteristics of the delay group postulated should be evident from the fact that the lifetime of thermal neutrons in an infinite medium of graphite is 12 msec. Using the term reflector-delayed neutrons, it is now appropriate to attempt to investigate the quantitative application of the notion to the KEWB experimental data.

C. SEVEN-GROUP INHOUR EQUATION

Incorporation of reflector-delayed neutrons as a seventh group into the six-group inhour equation

$$R = \frac{\omega \ell}{\sum_{i=1}^{6} \beta_i} + \sum_{i=1}^{6} \frac{f_i \omega}{\omega + \lambda_i}, \qquad \ldots(108)$$

where the terms have been defined above, can be performed by grouping the seventh group term with the lifetime

$$R = \frac{\omega}{\sum_{i=1}^{6} \beta_i} \left(\ell_o + \frac{\beta_7}{\omega + \lambda_7} \right) + \sum_{i=1}^{6} \frac{f_i \omega}{\omega + \lambda_i}, \qquad \ldots(109)$$

where ℓ_o is now adopted to designate the core lifetime.

Note that this equation has been divided by $\sum_{i=1}^{6} \beta_i$, so that the reactivity is in six group dollars as before. This is the least complicated of confusing alternatives, because the dollar unit, alghough defined $R = \rho k_{eff} / \sum_{i=1}^{n} \beta_i$ has become associated with the six groups of fission-product delayed neutrons, as has prompt critical. In terms of usage, it would be better to define the dollar by $R = \rho k_{eff} / \sum_{i=1}^{6} \beta_i$, and choose a new name for the case where the summation is over the index seven.

The form of Equation 109 is desirable because it associates the reflector-delayed neutron effect with the core lifetime, leaving the term involving fission product delayed neutrons unchanged. If Equation 109 is to fit the experimental inhour curve, then it must be identical to the six-group inhour Equation 108 for small ω, since the later is an adequate representation of the experimental results for long periods. Therefore, for $\omega << \lambda_7$,

$$\ell_o + \frac{\beta_7}{\lambda_7} = \ell \cong 62.5\,\mu\,\text{sec.} \qquad \ldots(110)$$

This value of ℓ is determined with the assumption that $\sum_{i=1}^{6} \beta_i = 0.008$.

Replacement of ℓ with $\ell_o + \beta_7/(\omega + \lambda_7)$ in the inhour equation can be seen to provide the type of roll-off manifested by the experimental inhour curve to the six-group curve, because the value of the term $\beta_7/(\omega + \lambda_7)$ continually decreases as ω approaches and passes the value of λ_7. The quantity $\ell_o + \beta_7/(\omega + \lambda_7)$ can be viewed as an effective neutron lifetime, $\ell(\omega)$, which becomes smaller as the reactor period decreases.

At any given value of the period, then, there is a value for $\ell(\omega)$ which will fit Equation 108 to the experimental inhour curve. If ℓ_o is known, and

$$\ell(\omega) = \ell_o + \beta_7/(\omega + \lambda_7) \qquad \ldots(111)$$

is rewritten as

$$\frac{1}{\ell(\omega) - \ell_o} = \frac{\omega}{\beta_7} + \frac{\lambda}{\beta_7}, \qquad \ldots(112)$$

a plot of the reciprocal of $\ell(\omega) - \ell_o$ against ω is a straight line with a slope equal to the reciprocal of β_7 and an intercept equal to λ/β_7. The latter condition is identical to that given by Equation 110. If ℓ_o is not known, one might expect that, since Equation 111 represents a functional dependence of $\ell(\omega)$ on ω, with three parameters ℓ_o, β_7, λ_7, measurement of $\ell(\omega)$ at three values of the inverse period would allow determination of the parameters. Simultaneous solutions of Equation 111 at three points, however, involve differences in the value of $\ell(\omega)$.

This magnifies the experimental error in $\ell(\omega)$ to the point of rendering computation of the parameters meaningless.

Since the core lifetime of the KEWB reactor has not been specifically measured, and in particular would be difficult to measure at the large values of k_{eff} employed in the reactor, the experimental data currently at hand is not sufficient to define a unique set of values for the reflector-delayed neutron parameters. The recourse at this point, then, is to calculate values for ℓ_o, β_7 and λ_7 from theory, if possible, and to employ the quantity judged to be most adequately predictable from theoretical considerations to obtain values of the remaining two parameters from the experimental data.

D. THEORETICAL VALUES OF REFLECTOR-DELAYED NEUTRON PARAMETERS

In addition to fulfilling the need for a theoretical value of one of the parameters ℓ_o, β_7 and λ_7 to determine the other two from the experimental inhour curve, the theoretical treatment should support the plausibility of the reflector-delayed neutron concept. That is, the reflector delayed neutron effect should be predictable from theory.

1. Mean Delay Time of Reflector Neutrons

The thermalization of the fast neutrons in the reflector followed by their diffusion and leakage will result in a thermal neutron distribution in the reflector. If the source of fast neutrons is instantaneously stopped at time t_o, then the flux as a function of position and time is given by

$$\phi(x,t) = \sum_n a_n \psi_n(x) e^{-(\bar{v} B^2 D + \bar{v}\Sigma_a)t}, \qquad \ldots(113)$$

where $\phi(x,D) = \Sigma a_n \psi_n(x)$ is the initial thermal flux expressed in terms of a set of orthogonal functions, $\bar{v}$ is the average velocity of the thermal neutrons, D is the diffusion constant, B_n is the buckling of the n^{th} neutron mode, Σ_a is the macroscopic absorption cross-section for neutrons of velocity $\bar{v}$, and a_n are arbitrary amplitude constants determined by the initial flux distribution.

Each mode of the flux decays with a time constant λ_n which is given by the bracketed quantities in the exponent of Equation 113. Therefore, the mean life for the n^{th} mode is:

$$\frac{1}{\lambda_n} = \ell_n = \frac{1}{\bar{v}(DB_n^2 + \Sigma_a)} \qquad \ldots(114)$$

The buckling of the reflector for the first mode can be computed from

$$B_n^2 = \frac{\int_V \nabla^2 \phi \, dv}{\int_V \phi \, dv} \qquad \ldots(115)$$

A two-group, two-region AIM 5 code calculation gives the value of the integrals in Equation 115. Evaluation of Equation 114 gives approximately 2 msec as the mean lifetime of thermal neutrons in the KEWB reflector. Only the first mode has been considered to be important in the reactor. Higher modes have been neglected because of the impossibility of running the reactor at sufficiently short periods to verify their presence.

2. KEWB Core Lifetime

It is desired to calculate the core lifetime of the reactor only, without incorporation of the delay time of neutrons thermalized in the reflector. The KEWB is a highly thermal reactor. Therefore one group theory gives a good approximation to the core lifetime,

$$\ell_{th} = \frac{\mathscr{L}_{th}}{v\Sigma_a} = \frac{1}{(1 + L^2B^2)} \frac{1}{v\Sigma_a}, \qquad \ldots(116)$$

where $\mathscr{L}_{th}$ is the thermal nonescape probability, $L^2 = D/\Sigma_a$, D is the thermal diffusion coefficient of the core, B^2 is the bare equivalent core buckling, v is the thermal velocity, and Σ_a is the thermal cross section of the core. Evaluation of Equation 116 for the KEWB underfull and full and full spherical cores yields values of 16 and 22 μsec, respectively. These values have been substantiated by more sophisticated computations with the AIM 5 and SOFOCATE codes, for $k_{eff} = 1.03$.

3. Reflector Delayed Neutron Abundance

Calculation of a value for β_7 has not been accomplished successfully at this time. A two-group, two-region code calculation has been performed with results indicating a value for the reflector-delayed neutron abundance which is much larger than that justifiable from experimental data because it includes the higher order modes of return. Multigroup, multiregion calculations are being undertaken in the attempt to compute the abundance of the individual modes. Actually, this effort should not be carried too far, because only the spatial aspect of the problem has been considered. Since a rigorous treatment should incorporate time and space, because it is not likely that the flux distribution in the core and reflector will remain constant throughout a transient, we can only rely upon the empirical success of the methods employed until a two-group, two-region space kinetics model has been evaluated.

E. VALUES OF REFLECTOR-DELAYED NEUTRON PARAMETERS

Using the computed value of $\lambda_7 = 500\ \text{sec}^{-1}$ to evaluate the other two parameters from the experimental in-hour curves gives $\beta_7 = 0.0228$ for both core loadings and values of the core lifetime nearly identical to the computed values of 16 and 22 μsec for the underfull and full cores respectively. If these values of the parameters are employed in the AIREK (see Section II.C) code together with appropriate void and temperature feedback equations, the type of holdup of power after the peak evidenced in Figure 8 is observed as the reactor period approaches 2 msec. Also, the pile oscillator data are fitted very well with values of the parameters very close to those mentioned here.[14]

F. EFFECT OF REFLECTOR-DELAYED NEUTRONS ON SAFETY

Presence of reflector delayed neutrons has a beneficial effect on the safety of KEWB type aqueous homogeneous reactors. This can be seen from comparison of the short period inhour equations with and without reflector delayed neutrons incorporated as a seventh delayed neutron group. The short period ($\omega >> \lambda_1$, 1 pertaining to the fission product delayed neutrons only) form of the KEWB inhour Equation 109 is

$$R = \frac{\omega}{\sum_{i=1}^{6} \beta_i} \left(\ell_o + \frac{\beta_7}{\omega + \lambda_7} \right) + 1, \qquad \ldots(117)$$

where $\beta_7 = 0.023$, $\lambda_7 = 500 \text{ sec}^{-1}$, and $\ell_o = 16 \mu\text{sec}$ for the underfull spherical core.

For no reflector-delayed neutrons, the inhour equation would be

$$R = \frac{\omega}{\sum_{i=1}^{6} \beta_i} \ell_o + 1. \qquad \ldots(118)$$

This equation would apply to the KEWB with no reflector, or with a reflector material having a thermal diffusion time within about an order of magnitude of the core lifetime; for example water. Under these conditions the value of ℓ_o, the core lifetime, would be shorter than for the reflected case because of the need for a higher uranium concentration with a less efficient reflector. A shorter lifetime favors the conclusions to be drawn from this comparison, but for simplicity let it be assumed that the value of ℓ_o is unchanged. Equations 117 and 118 with constant ℓ_o show that, for any given reactivity insertion greater than one dollar, the graphite reflected reactor does not go on as short a period transient as does the reactor with no reflector-delayed neutrons. For example, a 2-msec transient requires a \$3.4 reactivity insertion in the KEWB: this amount of reactivity would produce a 0.833-msec period in the reactor having no reflector delayed neutrons and the same core lifetime. Since it is necessary to load KEWB type research reactors to about 3% excess reactivity in order to permit irradiation of highly absorptive materials in the glory hole, it follows that accidental release of a large portion of this excess reactivity would produce a much milder transient with reflector delayed neutrons present.

The peak inertial pressure in the core increases approximately at the same rate as the peak power, both being proportional to the reciprocal period to the exponent 1.5. Potential danger to the reactor from the inertial pressure is therefore minimized by the presence of reflector-delayed neutrons, through their action to limit by as much as a factor of two the period produced by release of substantial amounts of excess reactivity.

VI. RAMP-INDUCED TRANSIENTS*

A series of transients was initiated by the withdrawal of one or more control rods at the normal startup rate, but with rod motion allowed to continue until after the maximum transient power had been achieved. The bursts produced by such ramp inputs of reactivity closely resemble those resulting from step-input transients whose period is the same as the minimum period observed in the ramp-induced case. With this classification, the largest ramp-induced transients produced in the KEWB reactor can be characterized as being in or slightly shorter in period than the prompt critical region. Radiolytic gas void is of negligible importance until well after the power peak in this period region. Reflector-delayed neutrons can be considered prompt for such periods, so that

$$\beta_{eff} \cong \sum_{i=1}^{b} \beta_i \text{ and } \ell = \ell_o + \frac{\beta_7}{\omega + \lambda_7} \cong \ell_o + \frac{\beta_7}{\lambda_7}.$$

Also, the return of fission product delayed neutrons can be neglected up to the time of peak power, so that the ramp-induced transients can be described up to the time of peak power by the space-independent kinetics equations in the form:

$$\frac{dN}{dt} = \frac{\beta_{eff}}{\ell}(R - 1)N \qquad \ldots(119)$$

$$R = R_1 At + \epsilon_1 E, \qquad \ldots(120)$$

where A is the ramp-rate of reactivity insertion, R_1 is a step input, if any, beginning the ramp, and the other symbols are defined as in Section III.

Combining equations yields

$$\frac{dN}{dt} = \frac{\beta_{eff}}{\ell}(R_1 + At + \epsilon_1 E - 1)N. \qquad \ldots(121)$$

*Most of this section was written by O. L. Hetrick. SPERT personnel have performed a similar analysis.[17]

Since the reciprocal period is the logarithmic derivative, we have

$$\frac{dN}{dt} = \omega N \qquad \ldots(122)$$

and

$$\omega = \frac{\beta_{eff}}{\ell}(R_1 + At + \epsilon_1 E - 1), \qquad \ldots(123)$$

from which

$$\frac{d\omega}{dt} = \frac{\beta_{eff}}{\ell}(A + \epsilon_1 N). \qquad \ldots(124)$$

This last equation is often written

$$\frac{d\omega}{dt} = a - bN \qquad \ldots(125)$$

where

$$a = \beta_{eff}\frac{A}{\ell}$$

and

$$b = -\beta_{eff}\frac{\epsilon_1}{\ell}.$$

Equations 122 and 125 may be combined to yield

$$\frac{dN}{d\omega} = \frac{\omega N}{a - bN} \qquad \ldots(126)$$

which integrates to

$$a \ln \frac{N}{N_o} - b(N-N_o) = \frac{1}{2}\left(\omega^2 - \omega_o^2\right) . \qquad \ldots(127)$$

It is always possible to choose the time associated with the subscript zero so that this equation becomes (approximately):

$$a \ln \frac{N}{N_o} - bN = \frac{1}{2}\omega^2 . \qquad \ldots(128)$$

At peak power, $\omega = 0$; hence

$$a \ln \frac{\hat{N}}{N_o} - b\hat{N} = 0 . \qquad \ldots(129)$$

At minimum period, Equation 128 becomes

$$a \ln \frac{N_m}{N_o} - bN_m = \frac{1}{2}\omega_m^2 . \qquad \ldots(130)$$

Equations 129 and 130 may be combined, eliminating N_o and resulting in

$$\omega_m^2 = 2a\left(\frac{\hat{N}}{N_m} - 1 - \ln \frac{\hat{N}}{N_m}\right) \qquad \ldots(131)$$

which, since $a = \beta_{eff} A/\ell$, may be solved for the neutron lifetime in terms of measurable quantities,

$$\frac{\ell}{\beta_{eff}} = \frac{2A}{\omega_m^2}\left(\frac{\hat{N}}{N_m} - 1 - \ln \frac{\hat{N}}{N_m}\right) . \qquad \ldots(132)$$

The time of minimum period is characterized by $d\omega/dt = 0$.

Hence Equation 127 becomes

$$N_m = \frac{a}{b} = -\frac{A}{\epsilon_1} . \qquad \ldots(133)$$

It may be noted that the original Fuchs model, on which this development is based, is slightly less general, since the equation corresponding to Equation 121 was written simply as

$$\frac{dN}{dt} = \frac{\beta_{eff}}{\ell}(At + \epsilon_1 E)N \ . \qquad \ldots(134)$$

Equations 132 and 133 hold, provided that (1) the transient is fast enough so that the emission of delayed neutrons is negligible, and (2) the energy coefficient of reactivity is constant.

The results of using Equations 132 and 133 on six of these experiments are shown in Table I. The value of β_{eff} assumed in computing ℓ was 0.008. The large uncertainty in ℓ and ϵ_1 is due to the difficulty of determining precisely the power at the time of minimum period. Nevertheless, the values of ℓ are remarkably consistent with the value 62.5 μsec implied by $\beta_{eff}/\ell = 128$ and $\beta_{eff} = 0.008$. The energy coefficient of reactivity determined in this way is in good agreement with the values obtained for step transients in this same period range.

TABLE I

RAMP TRANSIENTS IN KEWB

Initial Core Filling (%)	Ramp Rate* ($/sec)	Minimum* Period (msec)	Peak* Power (kw)	Power at** Minimum Period (kw)	Neutron** Lifetime (μsec)	Reactivity** Coefficient ($/Mw-sec)
85	0.079	133	933	181	56	0.44
85	0.119	77	2070	232	64	0.51
85	0.158	67	2400	272	63	0.58
100	0.068	98	1230	135	61	0.50
100	0.096	70	2340	196	65	0.48
100	0.126	57	3220	216	73	0.58

* 10% uncertainty
** 50% uncertainty

It is expected that this model would fail for faster transients (minimum periods in the msec range) when the more complex reactivity effects of gas voids

and reflector delayed neutrons become more important. Such transients would be of academic interest only, inasmuch as special high speed control rod drive mechanisms would have to be made to obtain greater ramp input rates. Step input transients, which can be thought of as infinite ramp rates, always provide the maximum size burst for a given total reactivity release. These provide a much more satisfactory means of evaluating the safety of the reactor in the case of release of large amounts of reactivity.

REFERENCES

1. J. W. Flora, ed. "Kinetic Experiments on Water Boilers, 'A' Core Report Part I, Program History, Facility Description, and Experimental Results," NAA-SR-5415.

2. R. Johnson, "Smooth and Differentiate Data Points," SHARE Number CL-SMDI, Lockheed Aircraft Corp., Calif. Div.

3. D. L. Hetrick and D. P. Gamble, "Transient Reactivity During Power Excursions in a Water Boiler Reactor, Paper 6-5 (ANS Winter Meeting December 8, 1958), and D. L. Hetrick's unpublished notes

4. A. Schwarz, "Generalized Reactor Kinetics Code AIREK," NAA-SR-Memo 3509 (January 1959)

5. D. L. Hetrick, "Velocity of Sound in Water Containing Gas Bubbles," AI-TDR-3148 (November 4, 1958)

6. D. P. Gamble, "A Proposed Model of Bubble Growth During Fast Transients in the KEWB Reactor," ANS Paper 25-3 (June 15, 1959)

7. W. H. Rodebush, "Nuclei in Evaporation and Condensation," Chemical Review, 44: p 269 (1949)

8. N. E. Harvey, W. D. McElroy, and A. H. Whiteley, "Cavity Formation in Water," Journal of Applied Physics, 18, p162-172 (February 1947)

9. F. E. Fox and K. F. Hersfeld, "Gas Bubbles With Organic Skin as Cavitation Nuclei," Journal of Acoustical Society of America 26: No. 6, p984-989 (1954)

10. M. Bloomfield, W. N. McElroy, R. E. Skinner, "Bubble Formation," a bibliography," NAA-SR-2551 (June 27, 1958)

11. D. L. Hetrick, M. S. Dunenfeld, A. Schwartz, "Numerical Computations for Fission Bursts in Pulsed Reactors," Paper 22-6 American Nuclear Society, Gatlinburg Tenn. (June 16, 1959)

12. H. B. Karplus, "The Velocity of Sound in Liquid Containing Gas Bubbles," COO-248 (June 11, 1958)

13. E. H. Kennard, "Radial Motion of Water Surrounding a Sphere of Gas in Relation to Pressure Waves," DTMB-516 (September 1943) David W. Taylor Model Basin

14. R. N. Cordy, "Kinetic Experiments on Water Boilers, "A" Core Report, Part III, Pile Oscillator Results, NAA-SR-5417 (December 1, 1960).

15. G. R. Keepin, T. F. Wimett, and R. K. Ziegler, "Delayed Neutrons from Fissionable Isotopes of Uranium, Plutonium, and Thorium," Physical Review Vol 107 (1957)

REFERENCES

16. Wimett, T.F., "Time Behavior of Godiva Through Prompt Critical," LA 2029 (May 11, 1956)

17. S.C. Forbes, F.L. Bentzen, P. French, J.E. Grund, J.C. Haire, W.E. Neyer, and R.F. Walker "Analysis of Self-Shutdown Behavior in the Spert I Reactor, IDO-16528 (July 23, 1959)